Mechanical Systems and Signal Processing 224 (2025) 111984

Contents lists available at ScienceDirect

Mechanical Systems and Signal Processing

journal homepage: www.elsevier.com/locate/ymssp

Early warning of structural damage via manifold learning-aided data clustering and non-parametric probabilistic anomaly detection

Alireza Entezami [a,*], Hassan Sarmadi [b], Bahareh Behkamal [a], Stefano Mariani [a]

[a] Department of Civil and Environmental Engineering, Politecnico di Milano, Milan, Italy
[b] Head of Research and Development, IPESFP Company, Mashhad, Iran

ARTICLE INFO

Keywords:
Structural health monitoring
Unsupervised learning
Manifold learning
Gaussian mixture model
Nearest neighbor graph
Probabilistic anomaly detection
Environmental variability

ABSTRACT

Unsupervised learning is an effective and practical methodology for structural health monitoring when the preparation of labeled training data regarding damaged states is intractable, unnecessary, and expensive. Despite several studies on this field, some challenging issues need further evaluations. The main objective of this research is to overcome the challenges concerning different variability patterns in unlabeled vibration data caused by single and multiple environmental and/or operational variations, non-generality of unsupervised learners in handling training data of different sizes, and impacts of false positive and false negative errors on early damage warning. A novel integrated unsupervised learning method is proposed that emanates from manifold learning-aided data clustering and non-parametric probabilistic anomaly detection. Data clustering is based on regularized Gaussian mixture modeling supported by nearest neighbor graphs, for which training data can be modeled on a manifold structure. The primary purpose of this step is to generate local subsets of the entire training data in an effort to minimize the effects of environmental and/or operational variations. A multi-fidelity hyperparameter optimization is also designed to set the main hyperparameters of the proposed clustering algorithm, namely the number of components (clusters) and a regularization value. Using the aforementioned local subsets, a non-parametric probabilistic anomaly detector is developed from a reverse Gaussian mixture function to compute anomaly scores for early damage warning. Modal frequencies regarding two large-scale bridges are used to validate the proposed method and compare it with some state-of-the-art techniques. Results confirm the effectiveness and reliability of this method with negligible errors under different environmental variability.

1. Introduction

A serious challenge in our modern society is to preserve civil structures that are of utmost importance to economic development, transportation networks, and energy supply. Different methodologies are sought to protect civil structures from any adverse change caused by damage, prior to any partial or even full collapse. In this regard, new technologies based on data-driven structural health monitoring (SHM) can be developed within the framework of artificial intelligence [1]. Exploiting various sensing systems [2,3], civil

* Corresponding author.
E-mail addresses: alireza.entezami@polimi.it (A. Entezami), hassan.sarmadi@alumni.um.ac.ir, sarmadi.ipesfp@gmail.com (H. Sarmadi), bahareh.behkamal@polimi.it (B. Behkamal), stefano.mariani@polimi.it (S. Mariani).

https://doi.org/10.1016/j.ymssp.2024.111984
Received 2 February 2024; Received in revised form 21 August 2024; Accepted 22 September 2024
Available online 4 October 2024

structures can be monitored intelligently by measuring static and/or dynamic responses under different excitations loadings. Measured responses are then handled to extract meaningful information, called damage-related features, and make a decision on the state of the structure being monitored [4].

The process of decision-making or feature classification in SHM are implemented in the three levels of early warning of damage (i.e., Has the structure suffered from any damage?), localization of damage (i.e., Where are the damaged components?), and quantification of damage (i.e., How severe is the localized damage?). The correct information and knowledge about early damage warning play significant roles in the next two levels. In fact, the success in damage localization and quantification depends on the effective and efficient early detection of damage. Compared with traditional visual inspections, an automated implementation of the first level of SHM can significantly expedite monitoring programs, reduce maintenance costs, improve structural safety, and prolong the lifespan of civil structures.

Within the paradigm of artificial intelligence, machine learning offers robust and effective approaches to early warning of structural damage [5–10]. The main criterion for selecting the best machine learning model among the supervised, semi-supervised, and unsupervised classes depends on the availability of labels for the training data. In the context of SHM, fully labeled training data needed for supervised learning contains structural features (e.g., modal frequencies) of both undamaged and damaged conditions, while unlabeled training data suitable for unsupervised learning is comprised of the only undamaged features. Partially labeled data related to semi-supervised learning refer to all the features regarding the undamaged condition, with a few available features regarding the damaged state [5]. For early damage warning, the collection of fully and partially labeled datasets is not trivial, as the current state of the structure is actually unknown and any method should make attempts to estimate it. On the other hand, it may not be logical to damage civil structures for preparing damage data. This conveys the great importance of unsupervised learning for the first level of SHM.

Anomaly detection (also termed novelty detection) is the main unsupervised learning method for decision-making or feature classification [11]. The purpose of an unsupervised anomaly detector is to develop a model or function via unlabeled data, and then determine an anomaly score (index) for each training or test sample. Finally, it can make a decision whether a test sample is an anomaly or a normal one. Various anomaly detectors based on statistical distances [12–14], statistical and probabilistic models [15–17], and deep neural networks [18,19] especially autoencoders [20–22], have been developed for early damage warning. Clustering-based anomaly detection is a recent improvement in unsupervised learning for decision-making; generally, this methodology leverages the concepts of hybrid and local learning algorithms [23]. To put it another way, a clustering-oriented anomaly detector consists of at least two steps of data clustering/partitioning and anomaly detection. In the first step, a clustering algorithm is used to split the entire training data into local subsets (clusters) in an effort to choose relevant training features and ignore irrelevant ones. In the second step, the selected local dataset provides the primary elements for developing a non-parametric or parametric anomaly detector. On this basis, the developed anomaly detector determines anomaly scores for all the training features, allowing to estimate a decision threshold. Finally, anomaly scores of test instances are compared with the estimated threshold for decision-making: if the anomaly score for a test sample exceeds the threshold, the anomaly detector warns about an abnormal (damaged) condition. Due to the coupling of data clustering and anomaly detection, different choices are available to develop clustering-aided anomaly detection techniques. Some examples of these approaches include the *k*-means clustering and Euclidean distance [24], agglomerative hierarchical clustering and multivariate Bhattacharyya distance [25], agglomerative concentric hypersphere clustering and Euclidean distance [26], Gaussian mixture model and Mahalanobis-squared distance (MSD) [27], spectral clustering and empirical anomaly indices [28], adaptive kernel spectral clustering and direct distance metrics [29], and hierarchical information clustering and density-based anomaly detection [30].

Despite the effectiveness and efficiency of clustering-aided anomaly detection, some challenges should still be dealt with properly. One of these challenges is related to the confounding influences caused by environmental and/or operational variability in SHM programs. This issue is crucial to SHM due to the deceptive effects of such variability conditions on decision-making, particularly in long-term monitoring [31]. On the one hand, changes in the environmental (e.g., temperature, humidity, wind speed and direction) and operational (e.g., excessive loadings and traffic) factors can alter structural responses similar to that linked to damage, leading to false positive errors. On the other hand, the level of variability of these conditions may be larger than damage, particularly compared to minor damage, masking the influence of damage and leading to false negative errors [17]. As the false positive and negative errors can be directly related to economic and safety issues, it is therefore essential to mitigate or remove the environmental and/or operational effects [31]. The other important issue pertains to the type of variability, as some specific environmental and/or operational factors are dominant. For example, daily and seasonal temperature fluctuations or freezing weather make single environmental variability conditions changing structural responses of short- and moderate-span bridges [32–34], while temperature, traffic, and wind are multiple environmental and operational factors simultaneously affecting structural responses of long-span cable-supported bridges [35,36]. This issue emphasizes the significance of developing robust methods with high generality investigated in this article. Further than the engineering challenges concerning the environmental and/or operational changes, the most significant technical issue is concerned with the limitation and complexity of some anomaly detectors in handling the aforementioned engineering issues under different sizes of the training features (e.g., small and large sets of modal frequencies obtained from short-term and long-term monitoring programs [16]). This is a demanding issue because some of these anomaly detection techniques are suitable for large data (e.g., anomaly detectors based on dimensionality reduction or feature selection strategies), but those may fail in yielding appropriate performances using small data and vice-versa. Thus, there is a critical need to develop a versatile and effective anomaly detection method capable of addressing the engineering and technical challenges associated with varying data scales.

This article proposes a new clustering-oriented anomaly detection method in an integrated unsupervised learning fashion. Initially, a novel manifold learning-aided clustering technique based on a regularized Gaussian mixture model (RGMM) supported by nearest

neighbor graphs (NNGs), called here RGMM-NNG, is proposed to split the entire training data into local subsets (clusters) regardless of the size of data. The main premise behind RGMM is that training samples can be modeled on a manifold structure, based on their NNGs, and regularization significantly aids this approach to enhance the clustering performance. Once the entire training dataset is clustered, its local subsets (features) are considered to develop a non-parametric probabilistic anomaly detector based on a reverse Gaussian mixture function (RGMF). The proposed anomaly detector, which is consistent with the Gaussianity assumption on the local subsets, is formed by handling the local training subsets, and its inverse is then used to compute anomaly scores for decision-making. Since the RGMM-NNG method conforms to a model-based parametric data clustering, this work presents a multi-fidelity hyperparameter optimization (MF-HPO) technique to determine the critical hyperparameters of RGMM-NNG, which are the optimal number of components (clusters) and a regularization value. In view of the importance of confounding influences related to the environmental and operational variations, the proposed MF-HPO technique is specifically designed with an emphasis on mitigating such conditions. The major innovations of this article are three-folds: (i) a novel integrated SHM method based on manifold-aided data clustering and unsupervised anomaly detection, (ii) a hyperparameter optimization approach for the RGMM-NNG, and (iii) a probabilistic non-parametric anomaly detector.

Different sets of dynamic features (i.e., modal frequencies), extracted from vibration data of two full-scale bridges, are used to assess the effectiveness and performance of the proposed method, and compare it with some state-of-the-art anomaly detection techniques. Results demonstrate that the proposed method is effective and reliable for SHM in the presence of single and multiple environmental/operational variations. As the local features extracted from the initial step of the proposed method can effectively mitigate the influences of environmental and/or operational variability on the whole data, RGMM-NNG significantly enhances the ability of RGMF to generate more discriminative anomaly scores. This results in superior outcomes in reducing false positive and negative errors compared to several state-of-the-art techniques.

2. Clustering-based anomaly detection method

The proposed method consists of two main steps: (i) data clustering via RGMM-NNG along with its hyperparameter tuning by means of MF-HPO, and (ii) density-based anomaly detection via RGMF. Fig. 1 shows the flowchart of the proposed method to summarize it. Accordingly, the method initially processes the training data points corresponding to the undamaged structural condition. These points are used to tune the number of clusters and the regularization value needed for RGMM-NNG. These hyperparameters enable the proposed clustering technique to properly subdivide the entire training points into optimum clusters, and then deal with the effects of the environmental and/or operational variability by yielding the minimum false positive error.

Subsequently, the local subsets obtained with RGMM-NNG, along with the training points, are exploited to develop the RGMF-based anomaly detector. In this regard, the mean vectors and covariance matrices related to the local subsets represent the main structure of the adopted anomaly detector. Training and test points are then handled to compute their anomaly scores, acting as damage indices. Within an unsupervised anomaly detection framework, the anomaly scores relevant to the training points are used to estimate a decision threshold, so that any deviation of the scores relevant to the test points gives a warning of damage. It is important to

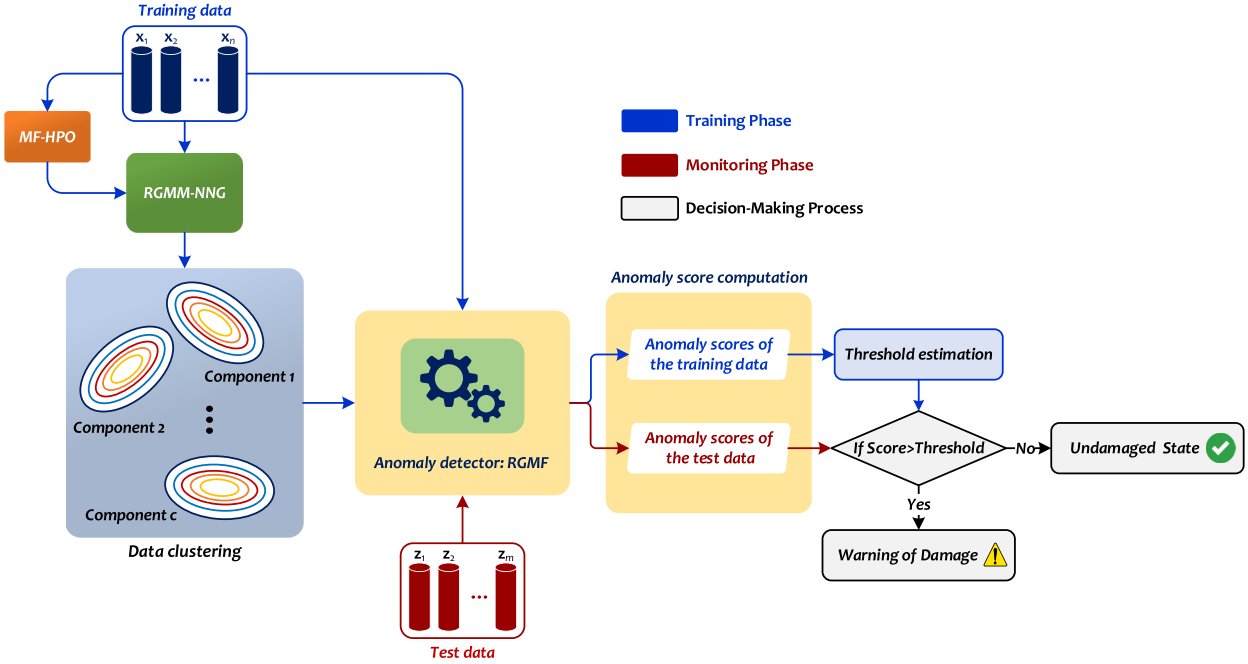

Fig. 1. Flowchart of the proposed clustering-based anomaly detection method.

acknowledge that the threshold estimation conducted during the training phase relies on an assumption that the structure being monitored is undamaged at that time. For the assessment of the current structural state during the monitoring stage, it is supposed that test samples become available in real time to perform online damage detection. Therefore, the test instances are successively processed by the trained anomaly detector to compute their anomaly scores.

2.1. Data clustering via RGMM-NNG

GMM is a probabilistic clustering method based on a weighted sum of Gaussian components. In this method, clustering is achieved by partitioning data samples into components, each of which is characterized by the mean vector, covariance matrix, and mixture weights, reflecting the Gaussian distribution of the data within that cluster [36: Chapter 9]. While GMM assumes that data distributions are supported in the Euclidean space [38], modeling in a submanifold, based on a manifold structure of data, can substantially enhance the learning performance.

The manifold of data is a mathematical structure that organizes data into a graph of connected regions where each data point is linked to a neighborhood set. Furthermore, a submanifold is a specific type of manifold situated within a higher-dimensional manifold [39: Chapter 16]. The manifolds and/or submanifolds can be used to represent a number of connected data points that can be given as transformations from a higher-dimensional space. In this context, manifold learning is an advanced machine learning algorithm that leverages these geometric structures to perform dimensionality reduction. By mapping high-dimensional data onto these manifolds or submanifolds, manifold learning aims to preserve the inherent data structures and relationships in the data. The process involves discovering the underlying manifold structure within the data and then representing this manifold in a new and lower-dimensional space. Since the manifold is often unknown, its structure can discretely be constructed by using a nearest neighbor graph. This approach offers a significant advantage by providing a more discriminative effect compared to traditional methods, relying on the Euclidean space [38]. On the other hand, it is important to acknowledge that manifolds are constructed from the training data related to the undamaged state. Utilizing the graph-based approach, a regular manifold is generated by ensuring that the training points maintain a coherent and consistent structure within the feature space, in spite of the presence of potential outliers.

By integrating the concepts of GMM-aided clustering and graph-based manifold learning, Liu et al. [40] suggested RGMM-NNG as a model-based clustering algorithm. This method incorporates a regularizer into the objective function of GMM, obtained by constructing an NNG and by applying the Kullback-Leibler (KL) divergence as a distance measure. The KL divergence on its own provides the distance between two probability distributions, so that the GMM problem can be solved more effectively than through the expectation–maximization algorithm [37: Chapter 9]. Compared to the traditional GMM, RGMM-NNG features a significant advancement thanks to the integration of NNG and KL divergence. This integration enforces a smoothness constraint rooted in the manifold structure, which enhances the capability of RGMM-NNG to accurately cluster complex data. Such advancements not only boost clustering precision, but also significantly improve the decision-making process in applications such as SHM. Despite the direct utilization of RGMM-NNG, this research presents important innovations. The primary innovation involves adapting RGMM-NNG to SHM for addressing one of the major challenges, i.e., the effects of environmental and operational variability. The other innovation lies in the integration of MF-HPO with RGMM-NNG, as detailed in Section 2.3, to optimally tune its critical hyperparameters including the number of clusters (components) and a regularization value. This strategic adaptation not only enables RGMM-NNG to provide local information for anomaly detection, but also emphasizes the mitigation of the environmental and operational impacts leading to improved detection accuracy.

Given a feature vector $\mathbf{x}_i$ relevant to the training matrix $\mathbf{X}\in\Re^{p\times n}$, where $i = 1,\ldots,n$, the main function for GMM is expressed as follows:

$$P(\mathbf{x}_i|\boldsymbol{\theta}) = \sum_{r=1}^{c} \omega_r G(\mathbf{x}_i|\boldsymbol{\mu}_r, \boldsymbol{\Sigma}_r) \tag{1}$$

where $P(\mathbf{x}_i|\boldsymbol{\theta})$ is the probability density function of the data point $\mathbf{x}_i$ given the model parameters $\boldsymbol{\theta}$; c denotes the total number of components of GMM; ω_r is the r^{th} mixture weight; and $G(\mathbf{x}_i|\boldsymbol{\mu}_r, \boldsymbol{\Sigma}_r)$ represents the Gaussian mixture density function of the r^{th} component, which is defined as:

$$G(\mathbf{x}_i|\boldsymbol{\mu}_r, \boldsymbol{\Sigma}_r) = \frac{1}{(2\pi)^{\frac{p}{2}}|\boldsymbol{\Sigma}_r|^{\frac{1}{2}}} \exp\left(-\frac{1}{2}(\mathbf{x}_i - \boldsymbol{\mu}_r)^T \boldsymbol{\Sigma}_r^{-1}(\mathbf{x}_i - \boldsymbol{\mu}_r) \right) \tag{2}$$

where $\boldsymbol{\mu}_r$ and $\boldsymbol{\Sigma}_r$ are the mean vector and covariance matrix of the r^{th} component; and $|.|$ represents the matrix determinant. The unknown elements of GMM are collected into $\boldsymbol{\theta} = \{\omega_r, \boldsymbol{\mu}_r, \boldsymbol{\Sigma}_r\}$. As already pointed out, GMM is therefore characterized by the mean vectors, covariance matrices, and mixture weights related to all components. The parameters in $\boldsymbol{\theta}$ are then estimated by the maximum likelihood method. Given the training data $\mathbf{X}$, the log-likelihood function of GMM is written in the following form:

$$\mathscr{L}(\boldsymbol{\theta}) = \log P(\mathbf{X}|\boldsymbol{\theta}) = \log \prod_{i=1}^{n} P(\mathbf{x}_i|\boldsymbol{\theta}) \tag{3}$$

where Π stands for the product operation. As Eq. (3) contains a nonlinear function of the unknown parameters in $\boldsymbol{\theta}$, the expectation–maximization algorithm can be exploited in an iterative manner [37: Chapter 9]. By introducing the conditional probability

distribution $P(r|\mathbf{x}_i)$, which represents the likelihood of the i^{th} feature vector belonging to the r^{th} component, the complete log-likelihood function is obtained as follows:

$$\mathscr{L}(\boldsymbol{\theta}) = \sum_{i=1}^{n} \sum_{r=1}^{c} P(r|\mathbf{x}_i)(\log\omega_r + \log G(\mathbf{x}_i|\boldsymbol{\mu}_r, \boldsymbol{\Sigma}_r)) \tag{4}$$

According to the expectation–maximization algorithm [41], the solution of Eq. (4) involves the expectation and maximization steps. The expectation step develops a function for the expected value of the log-likelihood, evaluated using the current estimates of the unknown parameters. The maximization step then calculates these parameters by maximizing this expected log-likelihood. In simpler terms, the expectation step in GMM computes the posterior probabilities of component points (memberships). Having considered the component-membership posterior probabilities as weights, the maximization step estimates the mean vectors, covariance matrices, and mixing proportions by applying the maximum likelihood. With such backgrounds, RGMM-NNG assumes that the conditional probability distribution $P(r|\mathbf{x}_i)$ can vary smoothly along the geodesics in the intrinsic geometry of $P(\mathbf{X})$, which represents the marginal probability distribution of the training matrix on the manifold structure. In other words, it is supposed that the conditional probability distributions of the feature samples resemble the marginal distribution of the training data on the manifold structure. This concept is known as the local consistency assumption [40].

To develop the objective function of RGMM-NNG, the similarity (distance) between two distributions is measured by the symmetric KL divergence. In this context, the application of the KL divergence is central to define the relationships within the NNG based on the distributional characteristics of the training points. Given the q-dimensional probability distributions $\widehat{P}_i = P(\mathbf{x}_i|\boldsymbol{\theta})$ and $\widehat{P}_j = P(\mathbf{x}_j|\boldsymbol{\theta})$ regarding the i^{th} and j^{th} samples of the training data, where $i,j = 1,\ldots,n$, the KL divergence is written as follows:

$$d_{KL}(\widehat{P}_i \| \widehat{P}_j) = \sum_{l=1}^{q} P(x_{il}|\boldsymbol{\theta}) \log\left(\frac{P(x_{il}|\boldsymbol{\theta})}{P(x_{jl}|\boldsymbol{\theta})}\right), \forall i \neq j \tag{5}$$

To avoid problems related to a non-symmetric measure, the symmetric version d_{SKL} of the KL divergence is introduced as:

$$d_{SKL}(\widehat{P}_i \| \widehat{P}_j) = \frac{1}{2}\left(d_{KL}(\widehat{P}_i \| \widehat{P}_j) + d_{KL}(\widehat{P}_j \| \widehat{P}_i)\right), \forall i \neq j \tag{6}$$

In the following, an NNG is derived from some nearest neighbors of the training samples. This describes a type of graph-based data structure, which is constructed from a set of training points in a metric space. Each point is connected to its nearest neighbors based on a specified distance metric. In the case of RGMM-NNG, the symmetric KL divergence is used as the metric to connect each training point to its nearest neighbors. The NNG can be modeled in undirected and directed configurations. Since the symmetric KL divergence ensures that the distance measure is the same in both directions, this symmetry implies that the graph considered in RGMM-NNG is undirected.

Based on the concept of manifold learning, the local geometric structure of the data can be effectively modeled by using the NNG on a scatter of training features. Let us consider a graph with vertices (nodes), each of which represents a training sample; if there are n training samples, the graph contains n vertices or nodes. The edges between the vertices are determined based on the nearest neighbor relationship. Specifically, an edge exists between two vertices i and j if either the vertex i is among the k-nearest neighbors of vertex j or vice versa. This bidirectional criterion ensures that the graph captures the local proximity or similarity between samples. Accordingly, one can derive an edge matrix, also referred to as an adjacency matrix [42], to represent the connections (edges) between the vertices (nodes) of the graph. This matrix is typically represented as a square matrix where both rows and columns correspond to the vertices of the graph. In other words, the entries of this matrix state whether a direct connection (edge) exists between the vertex corresponding to the row and the vertex corresponding to the column. Considering the i^{th} and j^{th} training samples, which is equivalent to the vertices i and j in the graph, the connectivity between these vertices in the edge matrix (γ_{ij}) is defined in the following form:

$$\gamma_{ij} = \begin{cases} 1, & \text{if} \mathbf{x}_i \in N_k(\mathbf{x}_j) \text{or} \mathbf{x}_j \in N_k(\mathbf{x}_i) \\ 0, & \text{otherwise} \end{cases} \tag{7}$$

where $N_k(\mathbf{x}_i)$ and $N_k(\mathbf{x}_j)$ denote the k-NNs sets associated with the training samples $\mathbf{x}_i$ and $\mathbf{x}_j$. Each entry in the edge matrix indicates the presence ($\gamma_{ij} = 1$) or absence ($\gamma_{ij} = 0$) of an edge between the vertices i and j. In this case, if $\mathbf{x}_i$ is among the k-NNs of $\mathbf{x}_j$ and vice versa, there is a connectivity between these samples and the edge entity corresponds to one. Once the edge matrix of the NNG is determined, the function related to the smoothness of $P(r|\mathbf{x}_i)$ on the graph is defined as:

$$\mathscr{R} = \sum_{i,j=1}^{n} d_{SKL}(\widehat{P}_i \| \widehat{P}_j)\gamma_{ij} \tag{8}$$

By adding this smoothness term to the log-likelihood function of GMM, one obtains:

$$\mathscr{K} = \mathscr{L} - \lambda\mathscr{R} = \sum_{i=1}^{n} \log \sum_{r=1}^{c} \omega_r G(\mathbf{x}_i|\boldsymbol{\mu}_r, \boldsymbol{\Sigma}_r) - \frac{\lambda}{2} \sum_{i,j=1}^{n} d_{SKL}(\widehat{P}_i \| \widehat{P}_j)\gamma_{ij} \tag{9}$$

where λ is the mentioned regularization parameter. The objective function of RGMM-NNG in Eq. (9) contains unknown parameters that can be estimated either internally within the algorithm or a priori using an additional technique. From a machine learning

perspective, the parameters estimated within the learning algorithm are referred to as model parameters; the other unknown parameters that significantly affect the overall performance of the learning process are called hyperparameters, and need to be tuned beforehand [43]. Accordingly, the mixture weights $\{\omega_1,\cdots,\omega_c\}$, the mean vectors $\{\boldsymbol{\mu}_1,\cdots,\boldsymbol{\mu}_c\}$, and the covariance matrices $\{\boldsymbol{\Sigma}_1,\cdots,\boldsymbol{\Sigma}_c\}$ are the model-parameters of RGMM-NNG estimated by the iterative expectation–maximization algorithm [40]. The method hyperparameters include the number of NNs (k), which contributes to build the NNG and determine the graph weights, the regularization value (λ), and the optimal number of components (c). Eventually, after determining the model and hyperparameters of RGMM-NNG, this method presents the components $\{\mathbf{C}_1,\ldots,\mathbf{C}_c\}$ along with their mean vectors and covariance matrices, serving as the main outputs of the first step of the proposed method. These outputs are then incorporated into the RGMF-based anomaly detector for early damage warning.

It is important to clarify the differences between the innovative application of RGMM-NNG and manifold learning presented in this study and the work by He and Guo [44]. This paper adopts the symmetric version of the KL divergence, while He and Guo [44] challenged the non-symmetric characteristic of the KL divergence and developed the RGMM using the Hellinger distance. Hence, the primary difference lies in the use of distinct distance measures. Moreover, another key distinction relates to the application domains of RGMM and manifold learning: specifically, the engineering problem in [44] focused on bearing health monitoring by addressing the dual challenges of constructing a proper health indicator and its suitability for predicting the remaining useful life of bearings. In contrast, this research aims to leverage the RGMM in conjunction with the NNG for data clustering to mitigate the effects of environmental and operational variability.

2.2. *Multi-fidelity hyperparameter optimization for RGMM-NNG*

Hyperparameter optimization is a critical process in learning any parametric model. This is due to the direct impact of hyperparameters on the model performance. In machine learning, this process can be performed by some well-accepted algorithms such as grid or random search, gradient-based optimization, Bayesian optimization, multi-fidelity optimization, and metaheuristic approaches [43]. When there is a small set of hyperparameters, model-free and multi-fidelity techniques are optimal solutions. In the context of the RGMM-NNG algorithm, it suffices to determine the number of components c and the value of the regularization parameter λ. Hence, MF-HPO is introduced to tune these elements before the final data clustering. Regarding the number of NNs, it is only necessary to provide the best NNG when all vertices are connected, which can be achieved by some empirical estimators. In this work, the empirical estimator proposed by Walters [45] is adopted, where for n data samples, k is given by the nearest integer to $0.4125\log(n)$. This means that the number of NNs necessitates a prior definition, without any incorporation into the MF-HPO algorithm. The flowchart of the proposed MF-HPO is depicted in Fig. 2.

According to the fundamental principles of the MF-HPO algorithms [43], the proposed strategy is carried out at multiple (two) levels. Initially, an attempt is made to optimize the hyperparameters within a large search space using a correspondingly large step

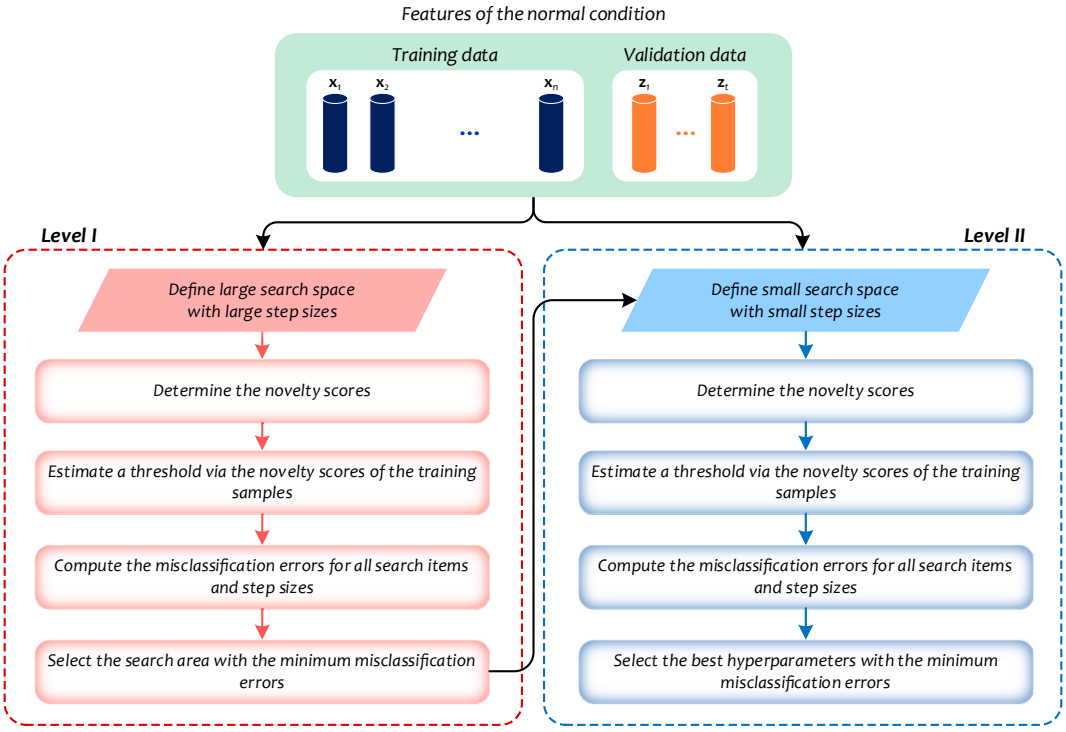

Fig. 2. Flowchart of the MF-HPO algorithm.

size. Subsequently, the outcomes from the first level are used to define a reduced search space and smaller step size, allowing the strategy for tuning the hyperparameters more precisely. Since c and λ should mitigate the negative effects of environmental and/or operational variations, the optimal criterion to set them is based on the minimization of the false positive rates. In this optimal solution, RGMM-NNG can thus split the entire training data into local subsets so that the confounding effects are minimized. As the data clustering step is implemented on the training data, which is related to the normal/undamaged structural state, the false positive error is the only available metric for the optimization criterion, which is defined as:

$$E = FP = \frac{N_{FP}}{N_{TN} + N_{FP}} \tag{10}$$

where N_{FP} and N_{TN} denote the numbers of false positive and true negative cases. Here, the terms "positive" and "negative" refer to the damaged and undamaged conditions [17]. Hence, the false positive represents the cases related to an undamaged structure, for which the anomaly detector incorrectly alarms in relation to the occurrence of damage; the true negative means instead that the structure is correctly detected in its normal condition by the anomaly detector. Apart from the false positive error, another evaluation metric for decision-making is the rate of false negative error, which is expressed as follows:

$$FN = \frac{N_{FN}}{N_{TP} + N_{FN}} \tag{11}$$

where N_{FN} and N_{TP} represent the numbers of false negative and true positive, respectively. In this regard, the false negative relates to a damaged structure, for which the anomaly detector mistakenly notifies no damage occurrence, while the structure is actually damaged. Conversely, the true positive means that the structure is accurately detected in its damaged condition.

2.3. Non-parametric probabilistic anomaly detection

Probabilistic anomaly detection is based on the estimation of the probability density or distribution function of data. It operates under specific assumptions about data distribution, such as Gaussianity, to define a threshold. Anomalies are detected by identifying data points that deviate significantly from the established assumptions [11]. The proposed anomaly detection method adheres to these foundational concepts, yet it employs innovative and distinct strategies. Initially, the proposed method generates a mixture of probabilistic models through the output of RGMM-NNG, which is the local mean vectors and covariance matrices related to the clusters of the training points, to derive a probabilistic function/model. The innovation of this strategy emanates from the theory of local learning, for which local information is applied to develop the anomaly detector, rather than customarily considering the probability density/distribution function concerning the entire training dataset.

Subsequently, the probabilistic model is inverted to define the RGMF and compute the anomaly scores of the training and test points. In the probabilistic anomaly detection framework, anomalies typically exhibit lower probability values compared to normal data points. This is attributed to the tendency of anomalies to change the statistical properties of normal data, notably by increasing the standard deviation and variance. Since the probability function is dependent on such statistical properties, the presence of anomalies leads to reduced probability values. This means that the anomaly detection process identifies anomalies by tracking a descending trend in probability values, where anomalies are characterized by the lowest scores. Despite the apparent reasonableness of this direct strategy for anomaly detection, it is less common in critical projects such as SHM of civil structures. This underscores the importance of establishing decision thresholds in crucial anomaly detection scenarios. Furthermore, the direct use of the minimum probabilistic scores limits the application of various threshold estimators, such as peak-over-threshold (POT) techniques relying on extreme value theory (EVT), which are only valid for maximum data distributions, for final decision-making. Accordingly, the proposed RGMF is represented by inverting the mixture probabilistic model, which is indicative of one of the main innovations presented for anomaly detection. The other key innovation is related to the non-parametric nature of RGMF that enables it to determine anomaly scores without any hyperparameter tuning. This underscores the simplicity and cost-effectiveness of the proposed anomaly detector.

The proposed RGMF is defined by exploiting the output of the RGMM-NNG algorithm, in terms of the local mean vectors $\{\boldsymbol{\mu}_1, \cdots, \boldsymbol{\mu}_c\}$ and covariance matrices $\{\boldsymbol{\Sigma}_1, \cdots, \boldsymbol{\Sigma}_c\}$. For any training sample, the anomaly score is obtained as follows:

$$\rho(\mathbf{x}_i) = \frac{1}{\max\limits_j \left(G\left(\mathbf{x}_i \middle| \boldsymbol{\mu}_j, \boldsymbol{\Sigma}_j \right) \right)} \tag{12}$$

where $i = 1,\ldots,n$ and $j = 1,\ldots,c$, and $G\left(\mathbf{x}_i \middle| \boldsymbol{\mu}_j, \boldsymbol{\Sigma}_j \right)$ is the probability distribution function defined in Eq. (2). Utilizing all the n samples collected during the training phase, the corresponding n anomaly scores relevant to the undamaged state are established and subsequently adopted to estimate the threshold τ. Since the effects of the environmental and/or operational variability can be mitigated by using the RGMM-NNG method, the POT-aided EVT threshold estimator proposed by Sarmadi et al. [46], is considered here to define the threshold τ for final decision-making. This threshold estimator offers the advantage of circumventing model selection, specifically eliminating the need for extreme value distribution modeling and parameter estimation.

If $\mathbf{z}_l$ is the l^{th} test point to be evaluated in real time during the monitoring phase, with $l = 1,\ldots,m$, early damage warning can be implemented in an online fashion. The anomaly score $\delta(\mathbf{z}_l)$ is determined by inverting its density value $\rho(\mathbf{z}_l)$, where:

$$\rho(\mathbf{z}_l) = \frac{1}{\max_j \left(G\left(\mathbf{z}_l | \boldsymbol{\mu}_j, \boldsymbol{\Sigma}_j \right) \right)} \tag{13}$$

and:

$$G\left(\mathbf{z}_l | \boldsymbol{\mu}_j, \boldsymbol{\Sigma}_j \right) = \frac{1}{(2\pi)^{\frac{p}{2}} |\boldsymbol{\Sigma}_j|^{\frac{1}{2}}} \exp\left(-\frac{1}{2} \left(\mathbf{z}_l - \boldsymbol{\mu}_j \right)^T \boldsymbol{\Sigma}_j^{-1} \left(\mathbf{z}_l - \boldsymbol{\mu}_j \right) \right) \tag{14}$$

Whenever the anomaly score exceeds the threshold, the procedure triggers an early damage warning in the sense that the structure has undergone some degradation and the current structural state is classified as damaged. Conversely, if the anomaly score falls below the threshold, the structure is considered to be still behaving normally and it is classified as undamaged.

3. Validation via full-scale bridge structures

3.1. A post-tensioned concrete bridge

This structure known as the Z24 Bridge is one of the most famous benchmark models in the SHM community. It was built as a three-span post-tensioned concrete bridge and located along the A1 Bern-Zurich Highway in Switzerland. The bridge was demolished in 1998, to build a new bridge with a larger side span. The structure had a main span of 30 m, and two side spans of 14 m. Fig. 3 shows the side and top views, as well as a picture of this bridge. The superstructure of the Z24 Bridge consisted of a two-cell closed box girder with tendons in the three webs. Both the main piers were built as concrete diaphragms, fully connected to the superstructure.

A long-term continuous monitoring test was carried out to measure acceleration responses and environmental factors such as air temperature, humidity, wind speed and direction, and rain before the complete demolition. Realistic damage patterns were also

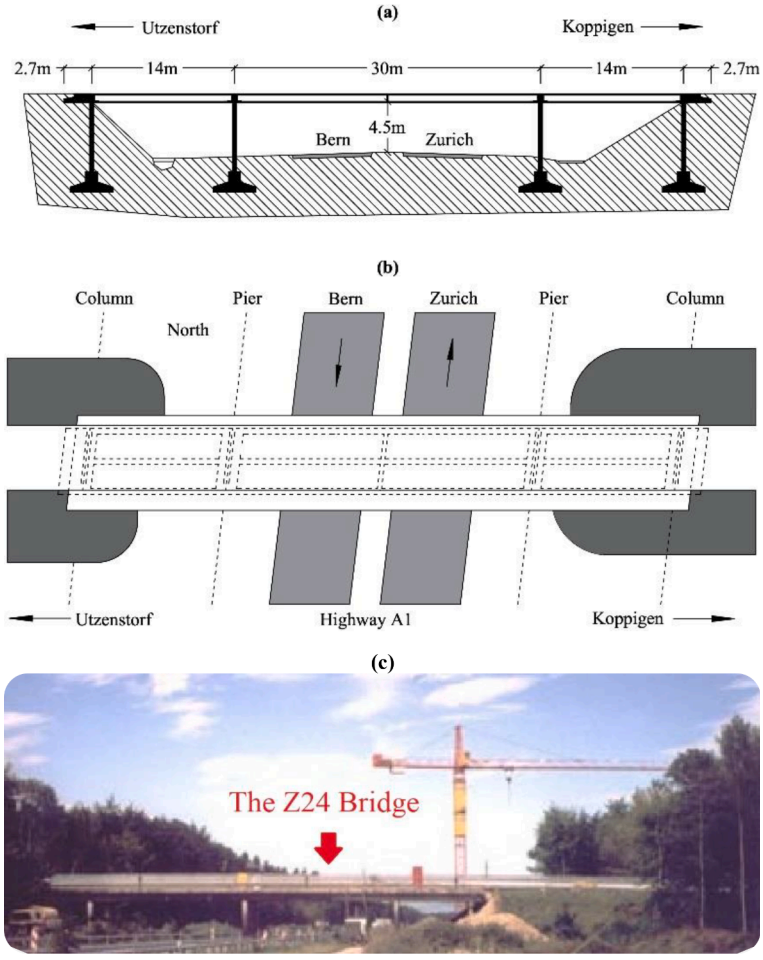

Fig. 3. Z24 Bridge: (a) Elevation view and main dimensions, (b) plan view, and (c) an old picture of the structure.

gradually introduced in a controlled manner, to define ad-hoc damaged conditions. An automated operational modal analysis based on the stochastic subspace identification was conducted by Peeters and De Roeck [47] to extract the one-year modal frequencies of the fundamental four vibration modes, as shown in Fig. 4. In this figure, the modal frequencies relevant to the first 3475 samples are associated to the normal or undamaged condition, while those relevant to the remaining samples 3476–3932 are instead related to the damaged state. An important insight provided by Fig. 4 is that the modal frequencies of the undamaged state exhibit sharp increases within the first 2000 samples. This is attributed to the impacts of freezing temperatures, which stiffened the bridge deck and resulted in abnormal frequency increases. Therefore, such single environmental variability linked to the freezing temperature is the major challenge in SHM of the Z24 Bridge.

To detect damage, 90% of the modal frequencies related to the normal condition are adopted to generate the training matrix $\mathbf{X}\in\Re^{4\times 3128}$, which therefore consists of 3128 feature vectors of four variables ($p = 4$). The remaining 10 % of the modal frequencies relevant to the normal condition, serving as the validation data, and all modal frequencies concerning the damaged state are instead used to assemble the test matrix $\mathbf{Z}\in\Re^{4\times 804}$. To start tuning the main hyperparameters of RGMM-NNG, the empirical estimator proposed by Walters [45] is initially applied to determine the number of NNs to construct the NNG and data manifold by considering the total number of training samples ($n = 3123$), leading to $k = 4$. Fig. 5 shows different three-dimensional (3D) views of the manifold structure of the training samples constructed from the NNG. This graph contains 3123 vertices (the blue circles), which are the training points and are connected by edges (the green lines) based on the four NNs of each point. The obtained NNG helps in understanding the relationships and proximities within the training data, which are essential for exploring the manifold structure indirectly.

In relation to the observed manifold structure, significant parallels can be drawn with transfer learning scenarios, particularly in the context of joint domain adaptation [48]. The manifold serves as a unified feature space that simplifies the representation of data from diverse structural states of the bridge, similar to how transformed feature spaces in transfer learning facilitate domain adaptation. This common feature space enables effective learning and generalization across varying structural conditions, which is similar to the methodology applied in other SHM applications conducted in [48]. Domain adaptation is particularly crucial for enhancing model transferability between different structural domains, which can accommodate significant variations in data distributions.

In the following, the proposed MF-HPO algorithm is adopted to set the other hyperparameters of the RGMM-NNG, i.e., the value of the regularization parameter (λ) and the number of components (c). Fig. 6 shows the results of this algorithm in terms of the maps of the false positive errors in the multilevel search spaces. In this figure, the vertical and horizontal axes represent the number of components and the regularization value, respectively. As shown in Fig. 6(a), the first level of the MF-HPO reveals that the lowest error rate is achieved with smaller values of both hyperparameters, ranging from 10 to 50 for c and from 0.01 to 0.1 for λ. These ranges are subsequently selected as the search area for the second level of the MF-HPO approach, as depicted in Fig. 6(b). The hyperparameters

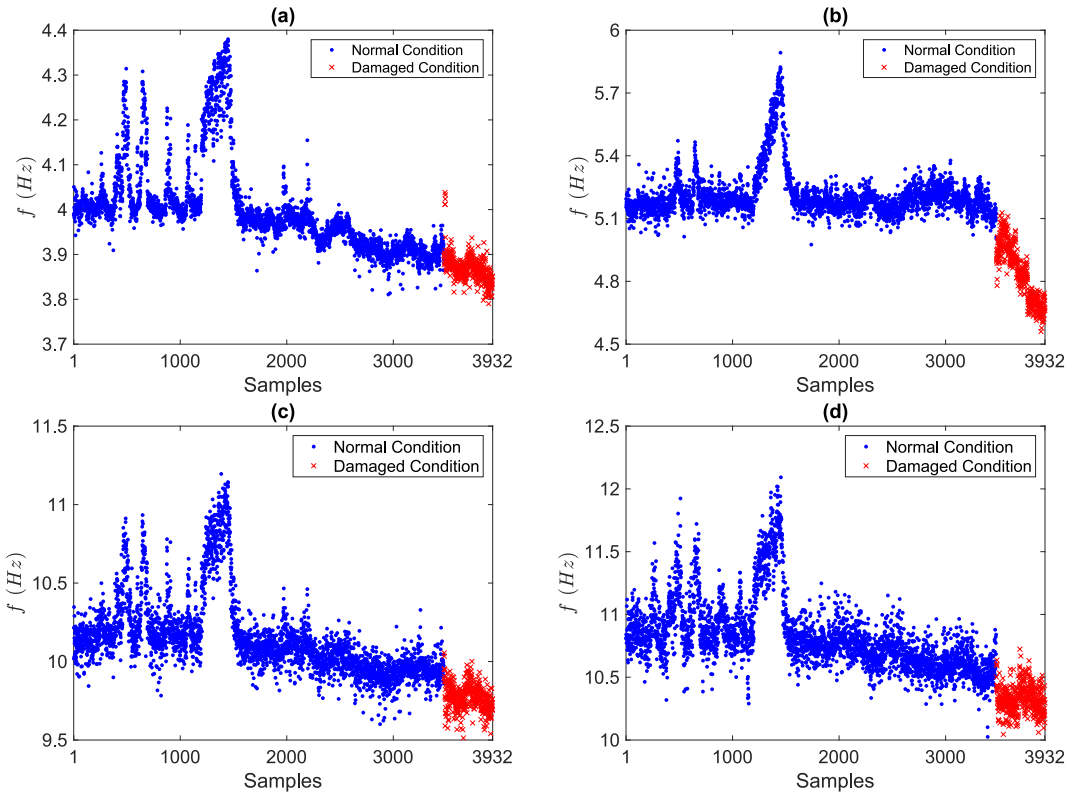

Fig. 4. Modal frequencies of the Z24 Bridge relevant to the first (a), second (b), third (c), and fourth (d) modes.

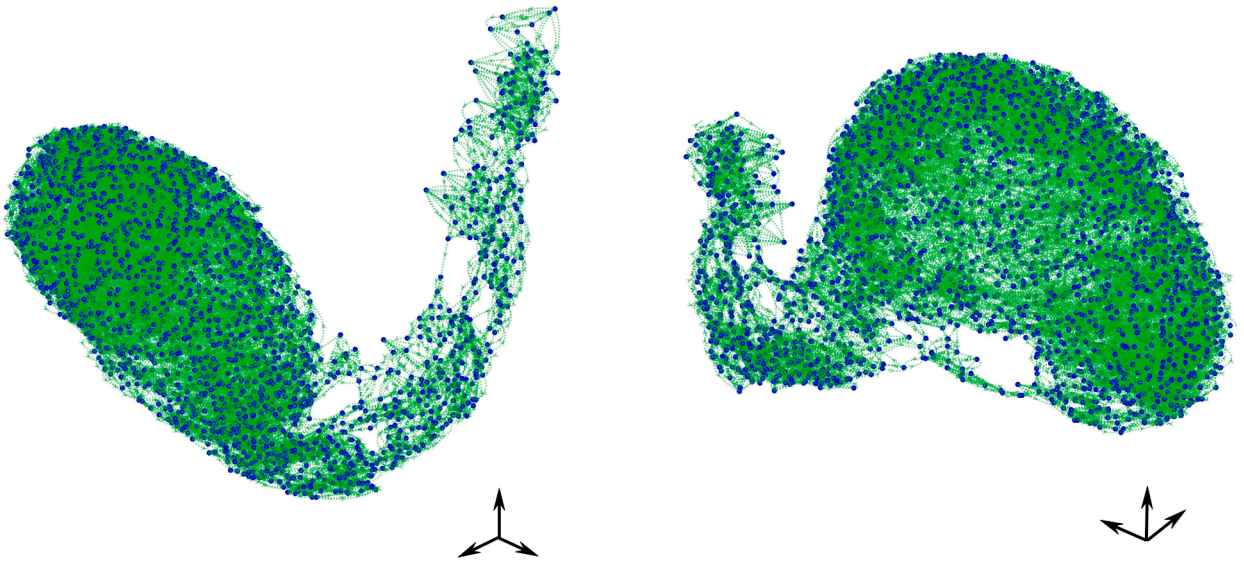

Fig. 5. Z24 Bridge: 3D views of the manifold of the training samples generated by the NNG with $k = 4$.

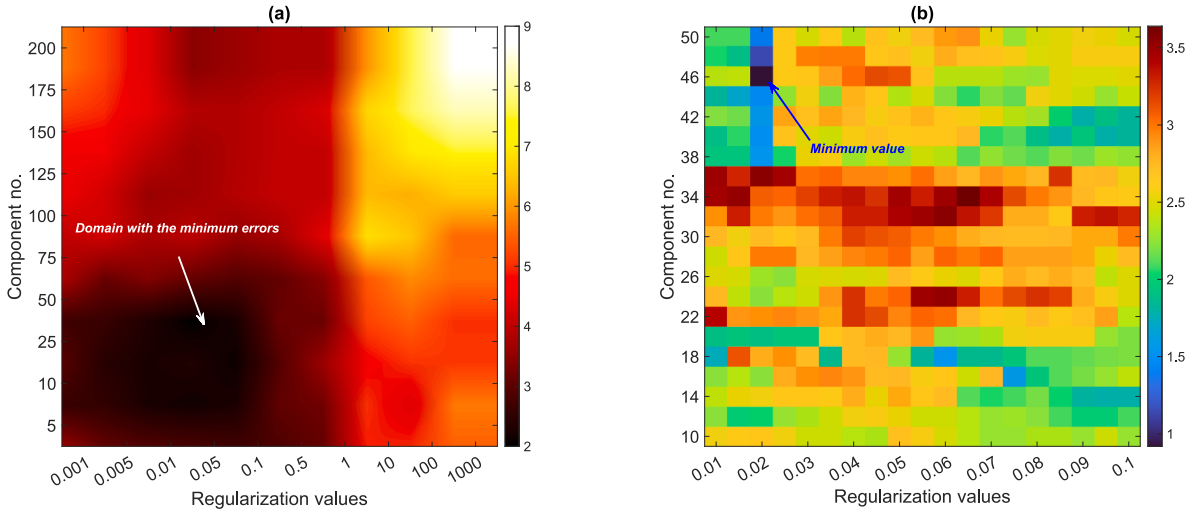

Fig. 6. Z24 Bridge: Maps of the false positive errors given by the proposed MF-HPO algorithm within the RGMM search space relevant to (a) Level 1, and (b) Level 2.

that lead to the minimum error rate in the second level are finally estimated as $c = 46$ and $\lambda = 0.02$. Therefore, the training samples are clustered into 46 components $\{\mathbf{C}_1,\ldots,\mathbf{C}_{46}\}$, to determine the corresponding mean vectors $\{\boldsymbol{\mu}_1,\cdots,\boldsymbol{\mu}_{46}\}$ and covariance matrices $\{\boldsymbol{\Sigma}_1,\cdots,\boldsymbol{\Sigma}_{46}\}$. The training and test samples (vectors) are then fed into the RGMF to determine their anomaly scores $\{\rho(\mathbf{x}_1),\ldots,\rho(\mathbf{x}_{3128})\}$ and $\{\rho(\mathbf{z}_1),\ldots,\rho(\mathbf{z}_{804})\}$.

By considering the anomaly scores of the training samples, an alarming threshold is estimated via the POT-EVT threshold estimator. Fig. 7 shows the result of damage detection obtained by the proposed RGMM-NNG-RGMF method, where the horizontal line refers to the estimated threshold (τ) and the vertical lines are used to distinguish the normal and damaged conditions in the training and monitoring phases. In Fig. 7, furthermore, the anomaly scores associated with the normal and damaged conditions are labeled as NC and DC, respectively. As can be seen in Fig. 7, the sudden jumps in the modal frequencies are no longer apparent in the anomaly scores of the training samples. This substantiates that the proposed RGMM-NNG technique generates proper local information (i.e., clustered training subsets), significantly filtering out the confounding influence of the considered environmental factor. This is because the data clustering mitigates internal variability within the clusters that enables the anomaly detector (RGMF) to focus more accurately on genuine data characteristics rather than fluctuations caused by the temperature variability. Accordingly, no false alarms are reported for the training samples, and the majority of the anomaly scores relevant to the validation data fall below the threshold, implying accurate detection of the normal condition. On the other hand, most of the anomaly scores relevant to the damaged state (i.e., the

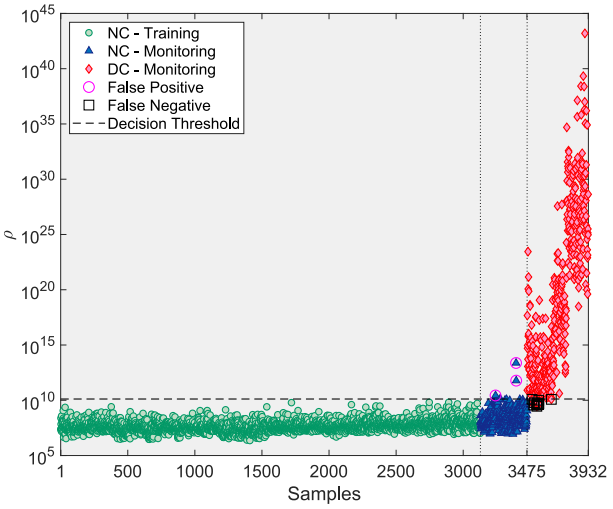

Fig. 7. Z24 Bridge: Early warning of damage via the proposed method.

samples 3476–3932) exceed the threshold, implying the correct detection of damage. Therefore, the proposed method succeeds in distinguishing the damaged state from the normal condition and filtering out the severe environmental variability to provide discriminative anomaly scores.

The performance of the proposed method is now assessed in the case of smaller training datasets, by decreasing the training ratio from 90% to 60% and 40% of the entire dataset, leading to the corresponding training matrices $\mathbf{X}_{60\%} \in \Re^{4\times 2085}$ and $\mathbf{X}_{40\%} \in \Re^{4\times 1390}$. The remaining 40% and 60% of the modal frequencies relevant to the normal condition, as well as all the modal frequencies of the damaged state are collected in the corresponding test matrices $\mathbf{Z}_{60\%} \in \Re^{4\times 1847}$ and $\mathbf{Z}_{40\%} \in \Re^{4\times 2542}$. Fig. 8 illustrates the results of early damage warning by adopting the same threshold estimator used in the reference case. It can be seen that the reduced number of training data significantly increases the number of false positive errors in the validation data. This increase is attributed to the fewer instances of training data available for allocation in data clustering, which impacts the ability of the proposed method to accurately discern between normal and anomalous conditions. Even if most of the anomaly scores concerning the damaged state fall above the threshold line, as Fig. 8(a) reveals, the rate of false negative errors increases compared to the corresponding error in Fig. 7. An important observation from Fig. 8(b) is that using only 40% of the normal features to assemble the training matrix fails in providing discriminative anomaly scores. As a result, the majority of the anomaly scores for the validation samples align with those of the damaged state, indicating an inability to effectively distinguish between the normal and damaged conditions using the 40% training ratio. To further assess the negative consequences of considering limited training data, Table 1 lists the number and percentage of false positive, false negative, and misclassification errors for all three training ratios. As expected, the best performance is linked to a relatively large training ratio (90%), while the method performance is seriously degraded in case of smaller training sets.

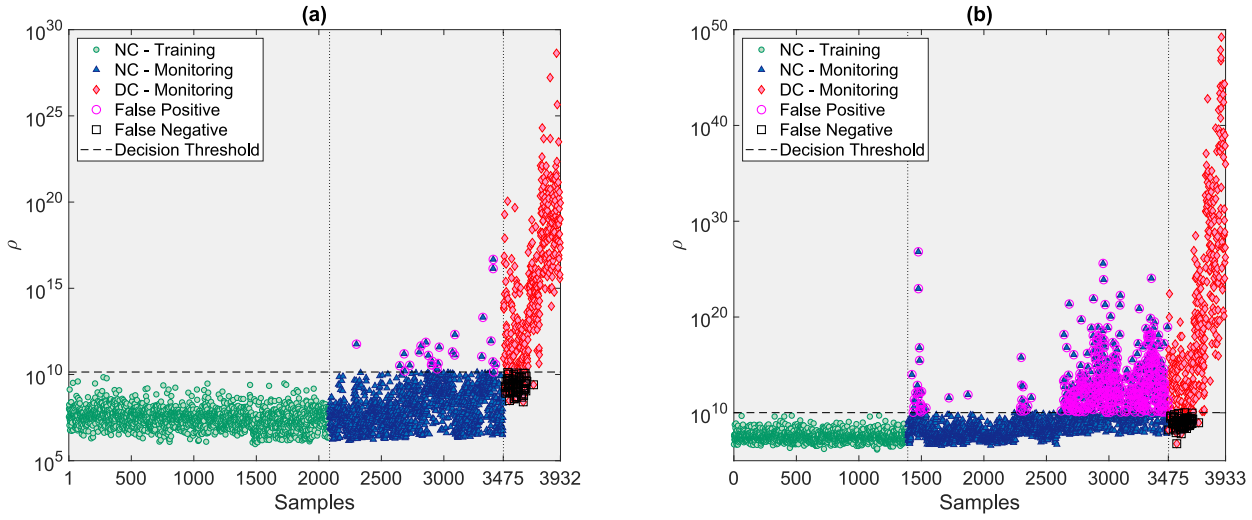

Fig. 8. Z24 Bridge: Early warning of damage via the proposed method by using smaller training rates: (a) 60%, and (b) 40%.

Table 1
Z24 Bridge: Performance assessment of the proposed method under varying training ratios.

Training ratios (%)	performance assessment		
	False positive	False negative	Misclassification
90	3 (0.09 %)	11 (2.41 %)	14 (0.35 %)
60	26 (0.74 %)	64 (14.03 %)	90 (2.28 %)
40	516 (14.84 %)	66 (14.47 %)	582 (14.80 %)

Having considered the reliable performance of the proposed clustering-aided anomaly detection method, a further evaluation is conducted to testify the impact of data clustering. For this purpose, the only RGMF anomaly detector is applied by incorporating the entire (original) training data. In this case, the mean vector and covariance matrix of $\mathbf{X}_{90\%} \in \Re^{4\times 3123}$ are estimated and used in RGMF. Fig. 9 illustrates the anomaly scores of the normal and damaged conditions of the Z24 Bridge using the complete training dataset incorporated into RGMF. Due to the presence of outliers (i.e., the environmental variability), which alter the statistical properties of the training data, it is evident from Fig. 9 that the direct application of RGMF cannot provide reliable outcomes for early damage warning in such a way that the sudden sharp increases in the original features is observable in the anomaly scores. Thus, the anomaly scores of the training points are either equal or even larger than some scores concerning the test samples.

Although the previous comparison emphasizes the importance of data clustering performed by RGMM-NNG to enhance damage detectability and reduce decision-making errors, it is necessary to further validate this importance by another anomaly detector. For this reason, the process of early damage warning in the Z24 Bridge is repeated by merging RGMM-NNG with the well-known MSD. Accordingly, the local mean vectors and covariance matrices obtained from RGMM-NNG are used to develop an MSD-based anomaly detector. For the i^{th} training feature, the anomaly score based on the MSD metric is given by:

$$d_M(\mathbf{x}_i) = \min_j \left(\left(\mathbf{x}_i - \boldsymbol{\mu}_j \right)^T \boldsymbol{\Sigma}_j^{-1} \left(\mathbf{x}_i - \boldsymbol{\mu}_j \right) \right) \tag{15}$$

The same holds for any test sample $\mathbf{z}_l$ by substituting it instead of $\mathbf{x}_i$. The other steps of the early damage warning are similar to those discussed for the RGMF-based anomaly detector. Fig. 10 shows the result of early damage warning by RGMM-NNG-MSD using the same POT-EVT threshold estimator. As can be seen, the proposed data clustering helps MSD to address the problem of severe environmental effects in the training samples so that no false positive errors emerge in the training phase. Moreover, most of the MSD-generated anomaly scores relevant to the damaged condition fall above the threshold, implying correct detection of damage. Comparing the RGMF and MSD through their anomaly scores, as shown in Fig. 7 and Fig. 10, it is evident that the use of RGMF results in fewer false positive and negative errors than MSD. More precisely, the rates of false positive, false negative, and misclassification errors in Fig. 10 are reported as 12 (0.34 %), 16 (3.50 %), and 28 (0.71 %), respectively. When these are compared to the corresponding errors listed for the proposed method under the 90% training ratio in Table 1, it can be demonstrated that RGMF reduces errors by 75%, 31.25%, and 50%, respectively, which highlight its efficacy in improving anomaly detection accuracy.

The proposed method is also evaluated against three state-of-the-art unsupervised anomaly detection techniques. Initially, the data clustering proposed in this study is compared with its original version, i.e., GMM, combined with the MSD metric for anomaly detection [49]. Subsequently, RGMM-NNG is assessed by partitioning the whole training features via the well-known *k*-means clustering (KMC) along with the Euclidean-squared distance (ESD) for anomaly score calculation [24]. Eventually, the proposed method is compared with a combination of PCA and MSD. In this approach, PCA provides normalized features by computing the residuals

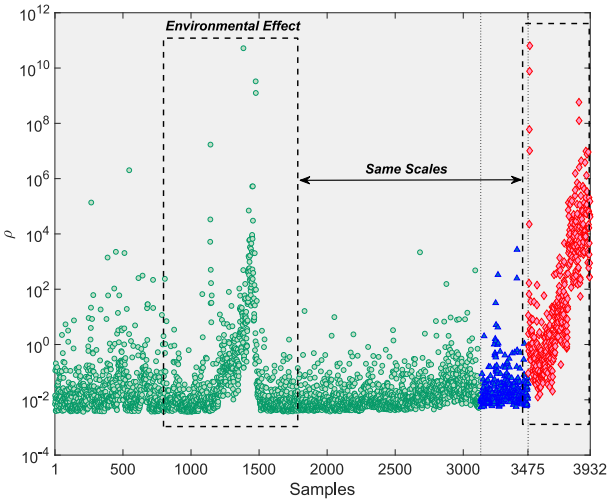

Fig. 9. Z24 Bridge: Early warning of damage via the RGMF-based anomaly detection over the entire training data (i.e., without the RGMM-NNG).

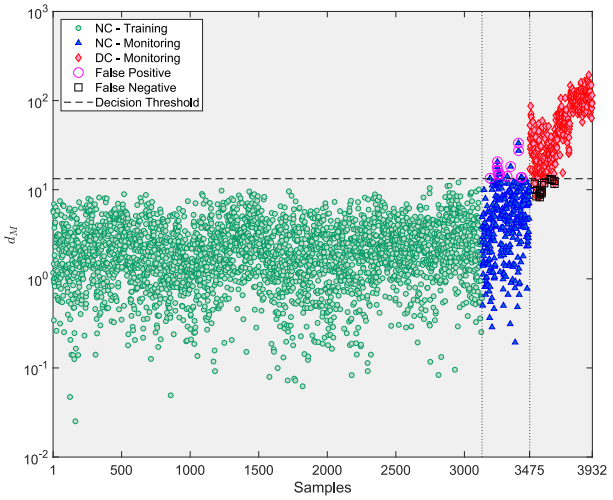

Fig. 10. Z24 Bridge: Early warning of damage by the RGMM-NNG-MSD.

between the original and reconstructed features obtained from the PCA model and MSD computes the anomaly scores [50]. Since both GMM and KMC are parametric techniques, the primary hyperparameters to be configured include the number of components for GMM and the number of clusters for KMC. These hyperparameters are optimized using the Bayesian information criterion (BIC) [23] and the Davies-Bouldin criterion (DBC) [51], respectively. For both approaches, the hyperparameters are determined by analyzing sample components and clusters and selecting those that yield the minimum BIC and DBC values. Fig. 11 shows the outcomes of the hyperparameter tuning for the GMM and KMC, where the optimal component and cluster correspond to 6 and 2, respectively, after 30 trials. Furthermore, the number of principal components, which is the only hyperparameter of PCA, is determined by the explained variance technique with a threshold set at 90 % [52], yielding two optimal principal components.

The results of early damage warning via these unsupervised learning techniques are shown in Fig. 12. In contrast to Fig. 7 regarding the proposed method, significant environmental effects still emerge in the anomaly scores relevant to the training samples. Moreover, half of the anomaly scores associated with the damaged state display the same range of values of the anomaly scores relevant to the normal condition, especially those highly affected by the environmental variability. As can be observed in Fig. 12(b) and (c), the worst performances belong to the KMC-ESD and PCA-MSD techniques. Therefore, it can be stated that the proposed method outperforms the state-of-the-art techniques aimed at early warning of damage and removing the severe environmental effects caused by freezing air temperature.

To summarize all the comparative studies, the receiver operating characteristic (ROC) and precision-recall (PR) curves of the various anomaly detection methods are plotted in Fig. 13. Concisely, an effective method is characterized by a ROC curve that approaches the upper-left corner of the ROC space and a PR curve that is near the upper-right corner of the PR space [50]. Conversely, an ineffective method exhibits a ROC curve close to the diagonal 45° line and a PR curve that aligns closely with the horizontal line. With these descriptions, it can be seen that the proposed RGMM-NNG-RGMF method shows the best performance with both the ROC and PR

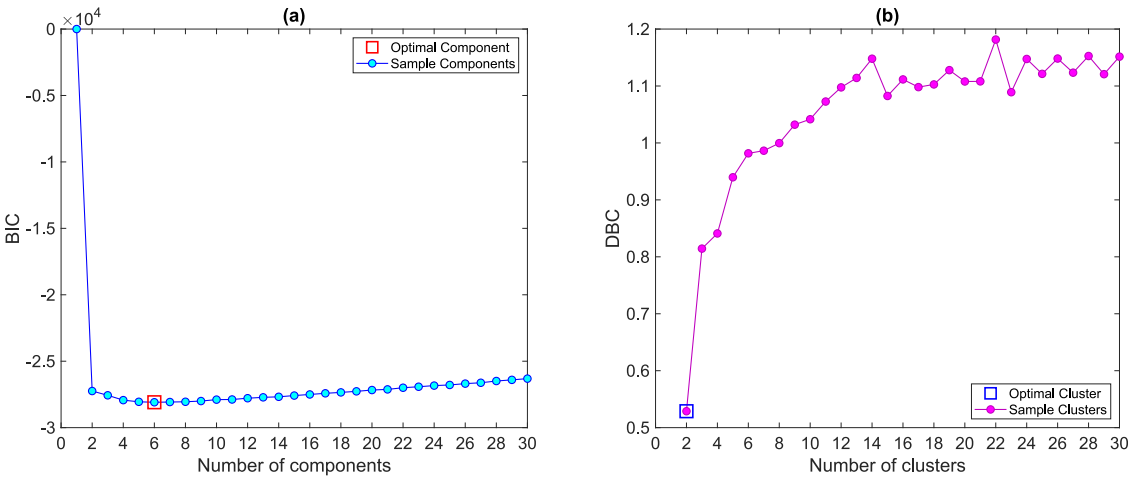

Fig. 11. Z24 Bridge: Hyperparameter optimization for the GMM and KMC based on the evolution of (a) the BIC and (b) the DBC values.

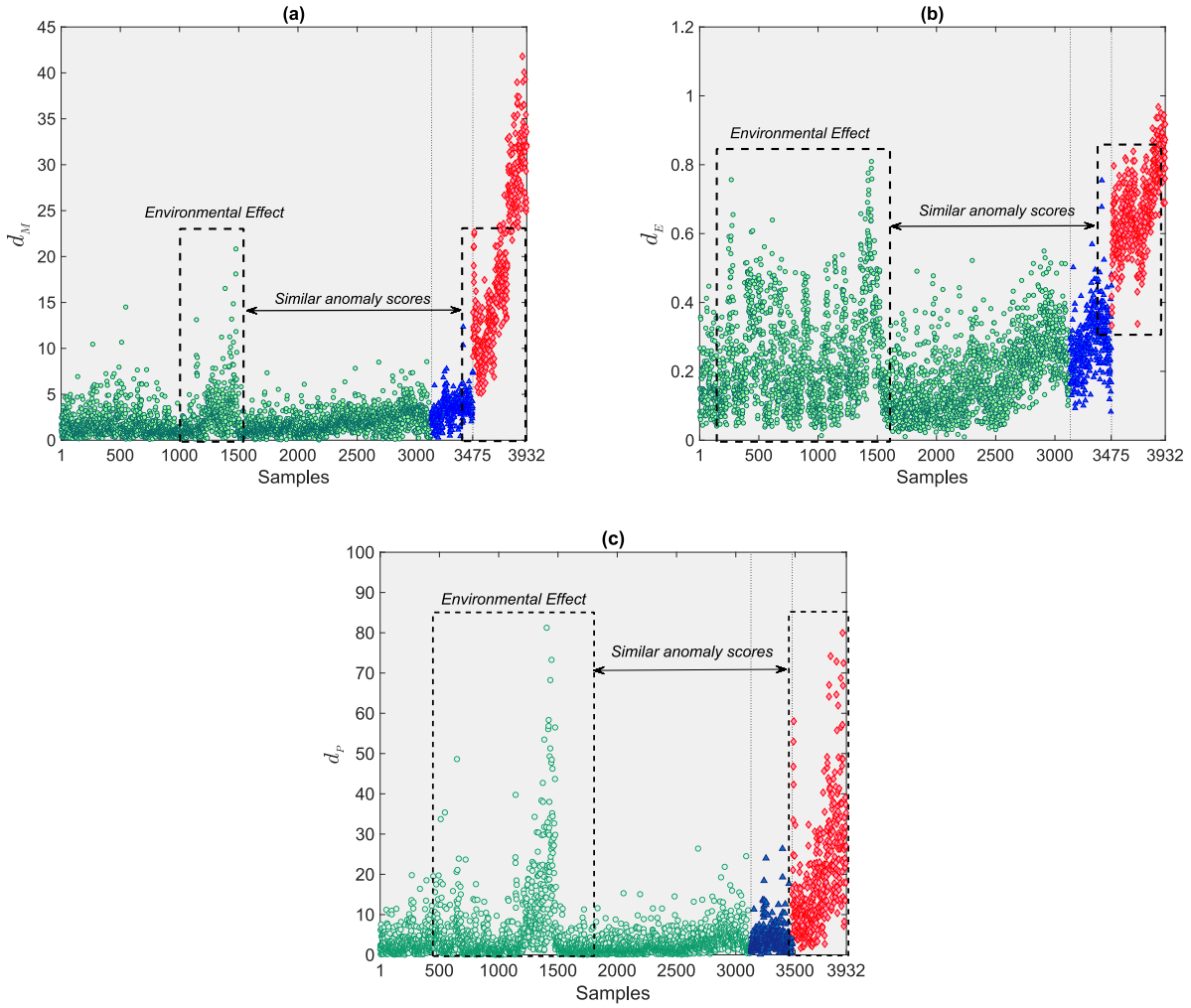

Fig. 12. Z24 Bridge: Early warning of damage via (a) GMM-MSD, (b) KMC-ESD, and (c) PCA-MSD.

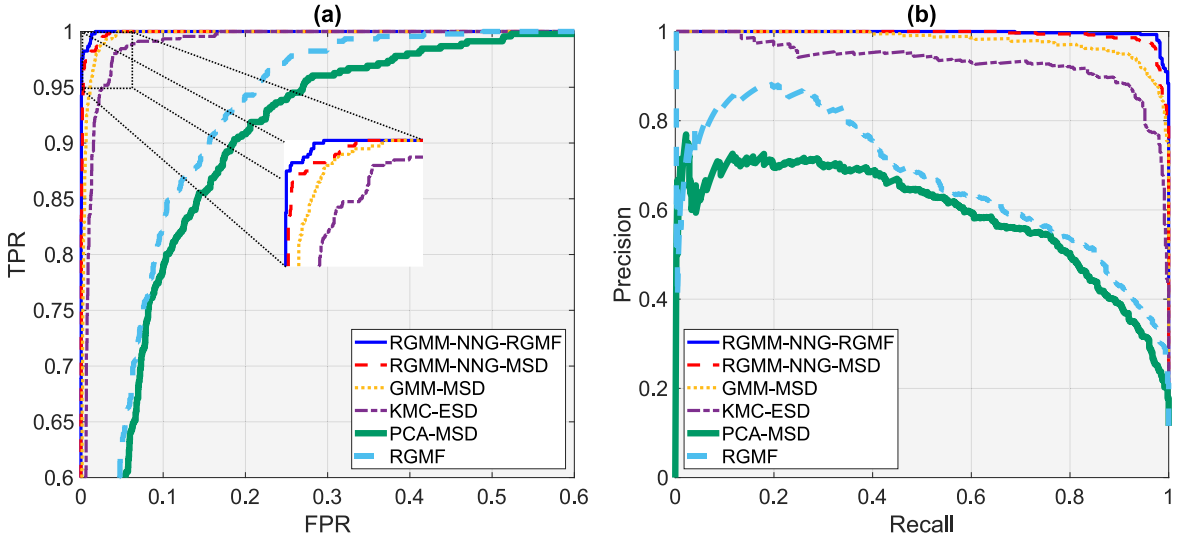

Fig. 13. Z24 Bridge: Performance evaluation of unsupervised anomaly detection methods via (a) ROC and (b) PR curves.

curves. This proves that it is highly effective for anomaly detection, and is characterized by high accuracy and a robust balance of false positive and true positive rates. In contrast, the PCA-MSD and RGMF techniques show the worst performances. While the RGMM-NNG-MSD, GMM-MSD, and KMC-ESD methods outperformed the PCA-MSD and RGMF, they still do not reach the effectiveness of RGMM-NNG-RGMF. An important conclusion drawn from Fig. 13 is that the clustering-aided anomaly detection methods are more successful than the other types of anomaly detection techniques, e.g., PCA-MSD and RGMF, due to the positive impact of data partitioning on the performance of the anomaly detector and on the removal of the variability effects.

Finally, the computational times of the various anomaly detection techniques are evaluated to assess their complexities in early damage warning using a relatively large feature dataset. This comparison has been conducted with a computer featuring a CPU Intel® Core i7, 64 GB of RAM, and Windows 10, utilizing the MATLAB 2023 built-in "tic-toc" function to measure the execution times. Table 2 lists the computational time (in seconds) for each step of the proposed and state-of-the-art anomaly detection techniques. It is important to note that the steps of hyperparameter optimization and data clustering are based solely on the training features, while the process of anomaly detection handles both the training and test instances. Accordingly, it is evident that the proposed RGMM-NNG-RGMF method requires substantial computational time. This increase is primarily due to the extensive search spaces considered in the double grid search algorithm of the proposed MF-HPO approach. Although the hyperparameter optimization strategies for GMM and KMC, which determine the number of components and clusters, take more time than the procedures of data clustering and anomaly detection, their execution times are shorter than those associated with the proposed MF-HPO algorithm. Among all the evaluated techniques, PCA-MSD provides the fastest analysis. Regarding the non-parametric anomaly detector functions, namely RGMF, MSD, and ESD, all exhibit fast performances. In summary, regardless of the effectiveness and reliability in early damage warning, for which the proposed method outperforms all the others, the current solution looks more complex than the others in the case of relatively large feature samples. This limitation can be mitigated by developing more efficient hyperparameter optimization strategies for RGMM-NNG.

3.2. A concrete cable-stayed bridge

This civil structure called the Yonghe Bridge [53,54] is a five-span concrete cable-stayed bridge constructed in China. Fig. 14 shows the side and top views, as well as a picture of this bridge. This structure has a main span of 260 m, and two side spans of 25.15 and 99.85 m as depicted in Fig. 14(b). The girder of the bridge consists of 74 precast segments formed continuously by cast-in-place joints, which linked the girder ends and formed transversely reinforced diaphragms. A total of 88 pairs of cables containing steel wires with the diameter of 5 mm were used to connect the towers to the bridge deck. In 2005, some serious cracks with a width up to 20 mm were detected at the bottom of the closure segment at the mid-span. Additionally, some cables near the anchors were reported as severely corroded. A repair program was then conducted from 2005 to 2007, to recast the mid-span girder and replace all of the stay cables [54]. In the meantime, a sophisticated SHM system was considered to measure the bridge response and some environmental data.

In August 2008, a crack at the left side span and a detachment between the girder and the piers at both side spans were detected during a regular inspection process. The vibration response acquired in the time window 2007–2008 can then be exploited to validate SHM methods [53]. The acceleration time histories measured by means of 14 single-axis accelerometers installed at the upstream and downstream sides of the bridge girder are here considered, according to the deployment configuration reported in Fig. 13(b). Regarding measuring the environmental data (i.e., wind and temperature), an anemoscope was mounted on the top of the south tower and a temperature sensor was installed at the mid-span of the girder.

The acceleration time histories of 13 accelerometers (i.e., excluding the 10th accelerometer due to meaningless values) recorded over the period from January 01 to July 31, 2008 are used to identify the bridge modal frequencies. This short-term monitoring program includes the measurements taken on nine specific days, i.e., January 01, January 17, February 03, March 19, March 30, April 19, May 05, May 17, July 31. According to Li et al. [53], the measurements acquired during the first eight days of the monitoring period mentioned above are representative of the bridge undamaged condition, while the last one (July 31st) is actually related to the damaged state. Using an operational modal analysis based on the frequency domain decomposition, see Sarmadi et al. [16], four stable modes were identified as main dynamic features of the bridge. Fig. 15 shows the time variation of the identified modal frequencies, where the first 192 samples are linked to the normal condition (i.e., 24 sets of accelerations for 8 days), and the last 24 samples are instead related to the damaged state. As the environmental factors recorded in terms of temperature and wind speed are not available, the interpretation of their effects is carried out via the aforementioned modal frequencies. Despite a clear gap between the frequencies of the normal and damaged state, which may simplify the process of anomaly detection, there are considerable variations in the modal frequencies of the normal condition. As discussed in Li et al. [35], the air temperature and wind speed had significant influences on the bridge modal frequencies. Since the low wind speed was dominant, the positive aerodynamic stiffness partially caused the jumps in the modal frequencies of the undamaged condition as can be observed in Fig. 15. Furthermore, some fluctuations (i.e., upward and

Table 2
Z24 Bridge: Assessment of computational times (sec) of the different stages of the anomaly detection techniques using relatively large feature samples.

Methods	Hyperparameter optimization		Data clustering	Anomaly detection	Total
RGMM-NNG-RGMF	600	780	15	4	1399
GMM-MSD	20		8	4	32
KMC-ESD	17		6	2	25
PCA-MSD	1		–	4	5

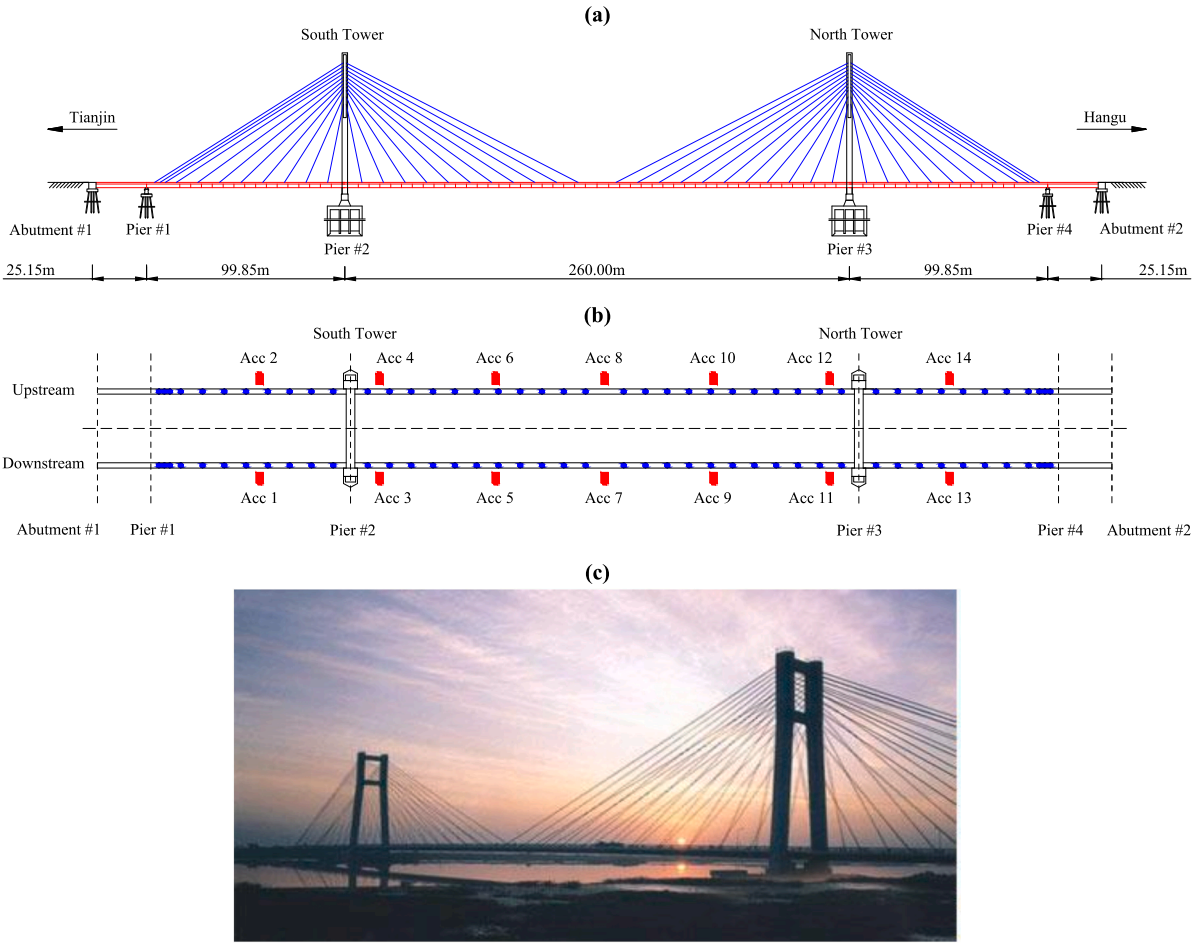

Fig. 14. Yonghe Bridge: (a) side view, (b) top view, and (c) a picture of the bridge.

downward of the bridge frequencies) are observable, which may be caused by the simultaneous impacts of daily temperature and traffic. In contrast to the Z24 Bridge, which is characterized by the single dominant environmental variability, the modal frequencies of the Yonghe Bridge were influenced by multiple environmental factors related to the air temperature and wind speed, and most likely by other unmeasured environmental and/or operational conditions.

To detect early damage in the Yonghe Bridge, 90% of the data relevant to the normal condition are used to assemble the training matrix $\mathbf{X}\in\Re^{4\times 172}$, which contains 172 feature vectors of the four vibration modes ($p = 4$). The remaining 10% of the data in the undamaged state, which serve as the validation data, and all the features relevant to the damaged state are collected in the test matrix $\mathbf{Z}\in\Re^{4\times 44}$. To perform data clustering via RGMM-NNG, the optimal number of NNs based on the Walters's estimator [45] turns out to be $k = 3$. Fig. 16 shows 3D views of the manifold structure built on the training samples. Due to the limited size of training data, which consists of only 172 samples, a single level of the MF-HPO technique is considered to tune the hyperparameters of the RGMM method. Hyperparameter ranges are set with the sample clusters between 1 and 20 and regularization values from 0.001 to 0.1. Optimal values are identified as $c = 10$ and $\lambda = 0.001$. Hence, the training samples are clustered into the ten components $\{\mathbf{C}_1,\ldots,\mathbf{C}_{10}\}$, with the local mean vectors $\{\boldsymbol{\mu}_1,\cdots,\boldsymbol{\mu}_{10}\}$ and covariance matrices $\{\boldsymbol{\Sigma}_1,\cdots,\boldsymbol{\Sigma}_{10}\}$, which are needed to model the RGMF-based anomaly detector for determining the anomaly scores of the training and test instances, i.e., $\{\rho(\mathbf{x}_1),\ldots,\rho(\mathbf{x}_{172})\}$ and $\{\rho(\mathbf{z}_1),\ldots,\rho(\mathbf{z}_{44})\}$, respectively.

Based on the outputs of data clustering through RGMM-NNG, Fig. 17 shows the result of early damage warning via the proposed method. For this purpose, the decision threshold is given by the same POV-EVT technique [46] adopted in the previous case. As can be discerned, no false alarm is reported for both the training and validation samples (i.e., labeled as "NC-Training" and "NC-Monitoring"). Moreover, all the anomaly scores relevant to the damaged state turn out to be greater than the threshold, without any false negative error. It can be thus concluded that the multiple environmental effects on the modal frequencies regarding the normal condition do not affect the obtained results. Due to a clear discrepancy between the anomaly scores relevant to the damaged and normal conditions, the proposed method consistently demonstrates its ability to provide reliable decision-making and accurate early damage warning. This is especially noteworthy as the proposed clustering-aided anomaly detection method could effectively handle a small set of dynamic features, despite their being influenced by multiple environmental/operational variations.

The performance of the proposed method is further evaluated by comparative analyses similar to previous structure. Fig. 18

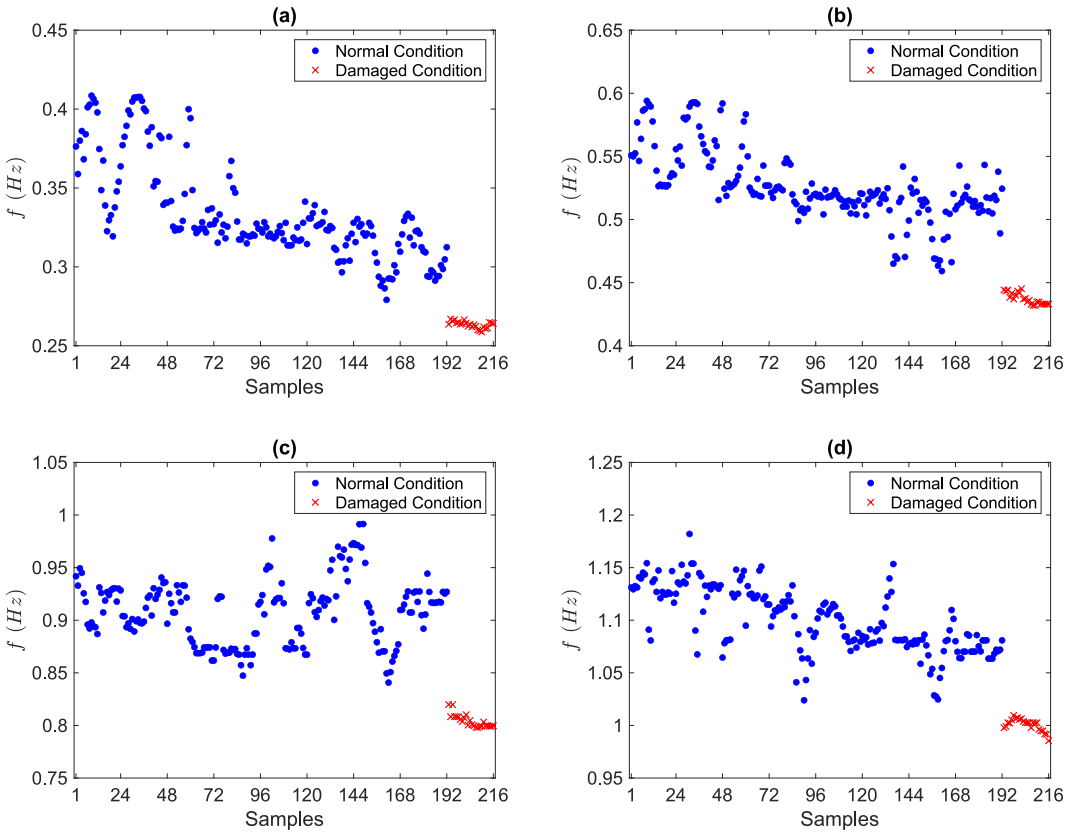

Fig. 15. Modal frequencies of the Yonghe Bridge relevant to the first (a), second (b), third (c), and fourth (d) modes.

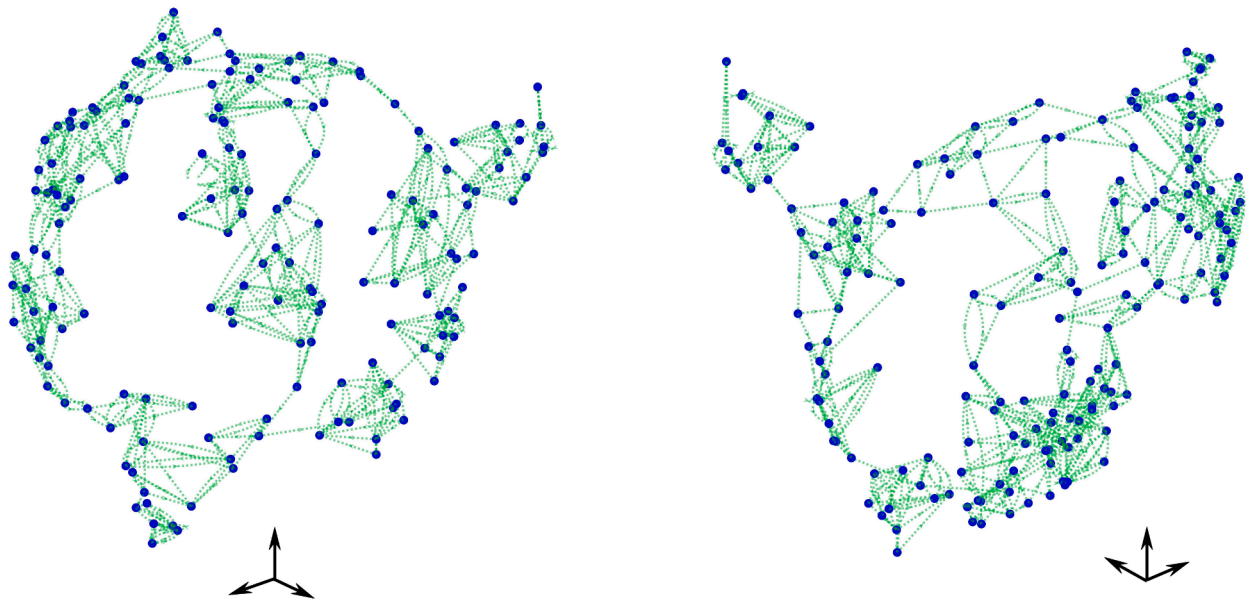

Fig. 16. Yonghe Bridge: 3D views of the manifold of the training samples generated by the NNG with $k = 3$.

illustrates the results of early damage detection in the Yonghe Bridge using the RGMF and RGMM-NNG-MSD. To better indicate the influence of data clustering and the use of local clustered training subsets, no threshold is allocated to indicate the outcome of the RGMF-aided anomaly detection displayed in Fig. 18(a). Hence, the single mean vector and covariance matrix derived from the entire

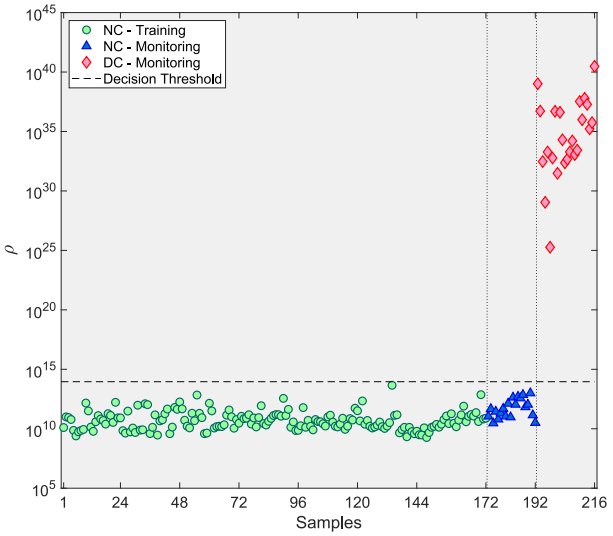

Fig. 17. Yonghe Bridge: Early warning of damage via the proposed method.

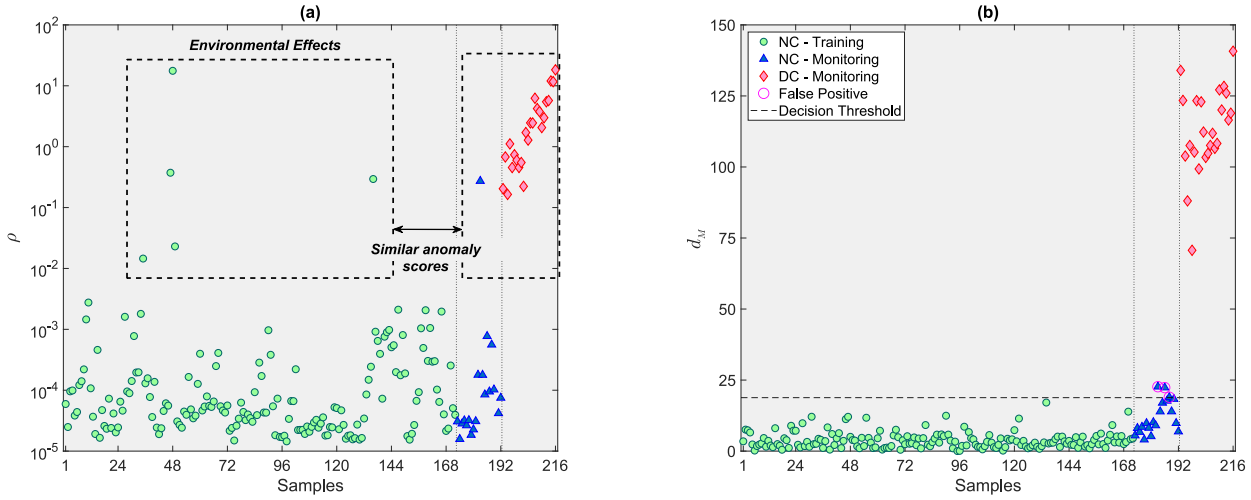

Fig. 18. Yonghe Bridge: Early warning of damage via (a) the RGMF-based anomaly detection using the entire training data (i.e., without the RGMM-NNG), and (b) the RGMM-NNG-MSD.

training data $\mathbf{X}\in\Re^{4\times 172}$ are utilized in the RGMF to determine anomaly scores for both the training and test points. As observed, the direct application of the RGMF alone is insufficient to address the effect of the environmental/operational variability. This is evidenced by the large anomaly scores for some training and validation samples, indicative of the undamaged condition, which match the scores from the damaged state. It should be noted that the emergence of such large anomaly values is the main reason for the decision to forgo any threshold in the decision-making process. In contrast, as Fig. 18(b) appears, the proposed data clustering technique significantly improves the conventional MSD-based anomaly detection to provide reliable early damage warning. Therefore, it can be concluded that local information obtained with RGMM-NNG can yield results more reliable than those obtained without any partitioning of the training data.

To directly assess the performances of RGMF and MSD, the observations in Fig. 17 and Fig. 18(b) indicate that the anomaly detector presented in this study is more effective than MSD. Despite their similar performances, the RGMF makes the final decision with fewer false positive errors compared to MSD in relation to the validation data (i.e., labeled as "NC – Monitoring"). Hence, the coupling of RGMM-NNG and RGMF leads to a more robust and effective tool for early damage warning under varying multiple environmental/operational conditions. The other comparative analysis investigates the proposed method with the state-of-the-art anomaly detection techniques GMM-MSD, KMC-ESD, and PCA-MSD. Fig. 19 depicts the BIC and DBC values of 20 sample trials for determining the optimal numbers of components and clusters for the GMM and KMC, which are identical to 13 and 8, respectively. Additionally, the explained variance technique is applied to determine the number of principal components for the PCA model, corresponding to 2.

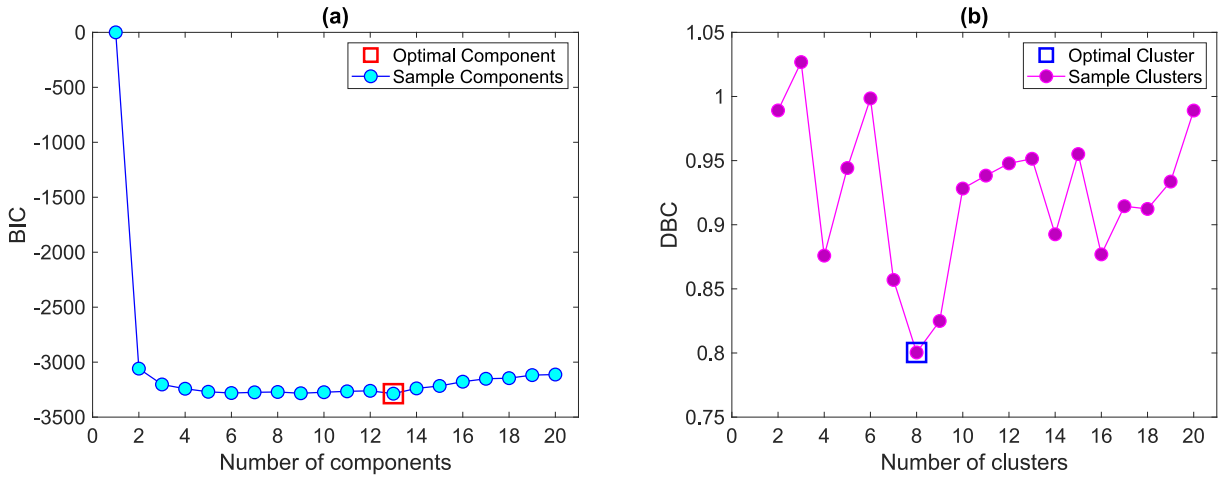

Fig. 19. Yonghe Bridge: Hyperparameter optimization for the GMM and KMC based on the evolution of (a) the BIC and (b) DBC values.

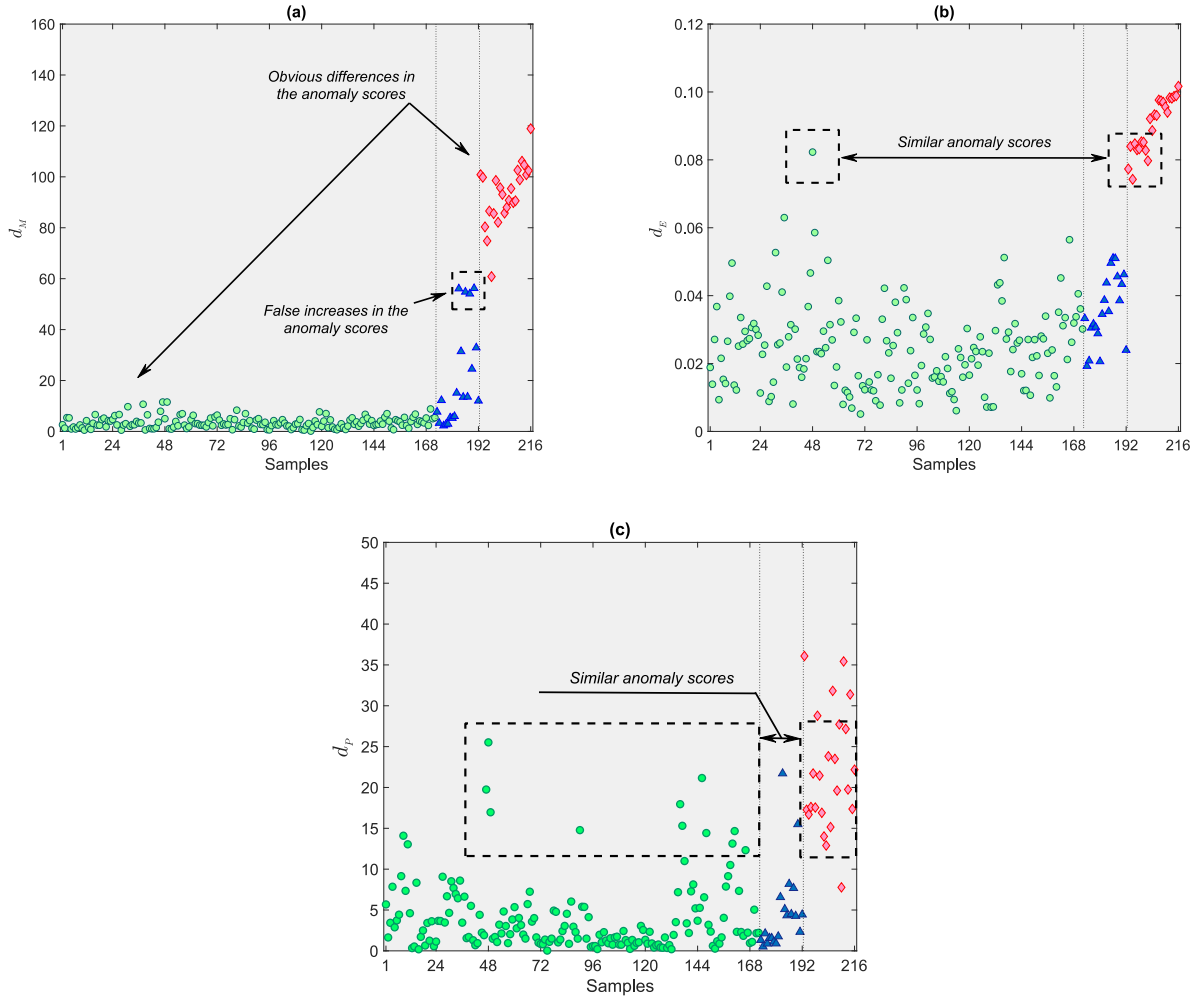

Fig. 20. Yonghe Bridge: early warning of damage via (a) GMM-MSD, (b) KMC-ESD, and (c) PCA-MSD.

Fig. 20 presents the results of early damage warning in the cable-stayed bridge using the aforementioned anomaly detection techniques. The method assessment in filtering the influence of the environmental/operational variability is based on the direct comparison of the anomaly scores of the training and test points.

In Fig. 20(a), it can be observed that the anomaly scores concerning the training samples, as provided by the GMM-MSD method, are roughly smooth without any considerable variability. Moreover, there is a clear difference between the anomaly scores relevant to the normal and damaged conditions. However, several anomaly scores linked to the validation data exhibit significantly increased values close to those of the damaged, leading to inaccurate assessment of the actual condition of the bridge. This outcome indicates the poor performance of GMM-MSD. In Fig. 20(b), the variability caused by the environmental and/or operational conditions are still visible in the anomaly scores relevant to the training/validation samples. Some anomaly scores linked to the normal condition take values in the same range of the scores related to the damaged state. This outcome is again indicative of the poor performance of KMC-ESD in providing discriminative anomaly scores and mitigating the influences of the multiple environmental/operational variations. As Fig. 20(c) reveals, the PCA-MSD exhibits the weakest performance among the considered techniques. This is primarily due to the significant reduction in the anomaly scores for the damaged state, which leads to a substantial overlapping of the scores between the undamaged and damaged conditions.

To summarize the performances of all anomaly detection techniques, Fig. 21 presents the accuracy rates for detecting damage in the cable-stayed bridge. A conventional threshold estimator based on a 95 % confidence interval is used to ensure a fair comparison across the techniques. This comparison reveals that the RGMM-NNG-RGMF method outperforms all the others, featuring the highest accuracy, while the PCA-MSD method shows the poorest performance. Although other techniques also outperform PCA-MSD, the proposed RGMM-NNG-RGMF consistently provides a superior effectiveness.

Eventually, Table 3 presents the computational times for different steps of the proposed and state-of-the-art anomaly detection methods using small vibration features. Compared to the computational times under relatively large feature instances related to the Z24 Bridge, the data in Table 3 reports a significant decrease in the computational demands for all methods, when applied to the Yonghe Bridge with a smaller number of feature samples. The complexity in the hyperparameter optimization and data clustering is notably reduced, which directly impacts the total computational time. However, the MF-HPO algorithm for tuning the main hyperparameters of RGMM-NNG still requires longer time compared with the hyperparameter tuning strategies for GMM, KMC, and PCA.

4. Conclusions

In this paper, an innovative clustering-based anomaly detection method has been proposed to warn early structural damage in the presence of single or multiple environmental and/or operational variability. This integrated unsupervised learning method has contained data clustering via RGMM-NNG and non-parametric density-based anomaly detection through RGMF. The MF-HPO algorithm has also been presented to tune the hyperparameters of RGMM. The proposed clustering technique has provided local clustered subsets from the training data to determine local mean vectors and covariance matrices to be used in RGMF. The modal frequencies of the Z24 and Yonghe bridges have been utilized to verify the effectiveness and reliability of the proposed method. Furthermore, several comparisons have been conducted to demonstrate the superiority of this method over some state-of-the-art techniques.

The main findings of this work can be summarized as follows. (1) The proposed RGMM-NNG-RGMF method has succeeded in dealing with the effects of single and multiple environmental/operational variability affecting the bridge modal frequencies. In the long- and short-term monitoring schemes with the different variability patterns, the proposed method could provide discriminative anomaly scores, without any adverse influences of the environmental and/or operational conditions. (2) Regardless of the threshold

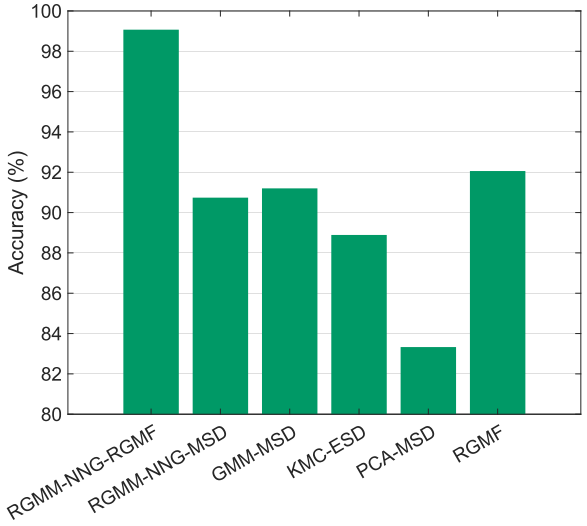

Fig. 21. Yonghe Bridge: Performance evaluations of the unsupervised anomaly detectors using the accuracy metric.

Table 3
Yonghe Bridge: Assessment of computational time (sec) of the different stages of the anomaly detection techniques, using small feature samples.

Methods	Hyperparameter optimization		Data clustering	Anomaly detection	Total
RGMM-NNG-RGMF	25	17	<1	<1	<43
GMM-MSD	<1		1	1	<3
KMC-ESD	<1		1	<1	<2
PCA-MSD	<1		–	1	<2

setting, it has been possible to clearly distinguish the damaged structural states from undamaged ones. This conclusion confirms the noteworthy ability of the proposed method to directly implement an early warning of damage without requiring threshold consideration, which is crucial in unsupervised anomaly detection scenarios. (3) The proposed MF-HPO algorithm has been shown suitable for hyperparameter tuning when the size of the feature dataset is relatively large. In case of a small dataset, e.g., that relevant to the Yonghe Bridge, a single level of MF-HPO has been shown to be sufficient. (4) The proposed RGMF anomaly detection has failed to provide correct anomaly scores for early damage warning in the absence of the RGMM-NNG technique. This emphasizes the importance of data clustering and local information derived from the entire training data, which is seriously influenced by the environmental and/or operational changes. (5) Under similar conditions and using the same technique for data clustering, RGMF has outperformed the well-known MSD. (6) The proposed method has proven superior to the state-of-the-art anomaly detection techniques GMM-MSD, KMC-ESD, and PCA-MSD. This superiority has been attributed to the ability of the proposed method to generate more discriminative anomaly scores, effectively addressing the environmental and operational effects. (7) The complexity assessment of the proposed and state-of-the-art anomaly detection techniques has indicated that RGMM-NNG-RGMF requires longer execution time, if compared to other methods. The extensive search spaces for the hyperparameters tuning of RGMM-NNG via the MF-HPO algorithm are the primary reason of the considerable computational burden of the proposed method.

In future research activities, the process of early damage warning can be extended by leveraging some advanced machine learning algorithms such as semi-supervised learning and incremental learning to design real-time SHM schemes with limited training data. Furthermore, while this study has focused on modal frequencies, which are widely-used and well-accepted vibration features for early damage warning, future research will concentrate on raw acceleration data. This shift will potentially eliminate the need for operational modal analysis techniques for modal identification.

Despite the effective performance of the proposed MF-HPO algorithm for tuning the main hyperparameters of RGMM-NNG, the major encountered limitation has been shown to be related to the computational intensity, particularly when large datasets are handled with large hyperparameter spaces. This issue stems from the iterative nature of the MF-HPO algorithm and the need to inspect multiple model configurations across different fidelity levels, that significantly prolongs the hyperparameter optimization process. To address this limitation in future studies, strategies will be employed to enhance the efficiency of hyperparameter optimization. These include adopting advanced search algorithms such as Bayesian and genetic optimizations, leveraging parallel computing, and implementing adaptive fidelity mechanisms.

CRediT authorship contribution statement

Alireza Entezami: Writing – original draft, Software, Methodology, Conceptualization. **Hassan Sarmadi:** Writing – review & editing, Software, Resources, Methodology, Conceptualization. **Bahareh Behkamal:** Writing – review & editing, Validation, Methodology. **Stefano Mariani:** Writing – review & editing, Validation, Supervision.

Declaration of competing interest

The authors declare that they have no known competing financial interests or personal relationships that could have appeared to influence the work reported in this paper.

Data availability

Data will be made available on request.

Acknowledgement

This research was partially funded by the European Union's Horizon Europe Research and Innovation Programme – NGI Enrichers, Next Generation Internet Transatlantic Fellowship Programme under Grant No. 101070125. The authors express their gratitude to MITACS organization in Canada, Prof. Ursula Eicker, Canada Excellence Research Chair in Smart, Sustainable, and Resilient Communities and Cities, and the Next-Generation Cities Institute at Concordia University, for their support on this research.

References

[1] O. Avci, O. Abdeljaber, S. Kiranyaz, M. Hussein, M. Gabbouj, D.J. Inman, A review of vibration-based damage detection in civil structures: From traditional methods to Machine Learning and Deep Learning applications, Mech. Syst. Sig. Process. 147 (2021) 107077.
[2] S. Sony, S. Laventure, A. Sadhu, A literature review of next-generation smart sensing technology in structural health monitoring, Struct. Contr. Health Monit. 26 (2019) e2321.
[3] H. Sarmadi, A. Entezami, K.-V. Yuen, B. Behkamal, Review on smartphone sensing technology for structural health monitoring, Measurement 223 (2023) 113716.
[4] C. Zhang, A.A. Mousavi, S.F. Masri, G. Gholipour, K. Yan, X. Li, Vibration feature extraction using signal processing techniques for structural health monitoring: A review, Mech. Syst. Sig. Process. 177 (2022) 109175.
[5] L.A. Bull, K. Worden, N. Dervilis, Towards semi-supervised and probabilistic classification in structural health monitoring, Mech. Syst. Sig. Process. 140 (2020) 106653.
[6] P. Gardner, X. Liu, K. Worden, On the application of domain adaptation in structural health monitoring, Mech. Syst. Sig. Process. 138 (2020) 106550.
[7] J. Gosliga, D. Hester, K. Worden, A. Bunce, On Population-based structural health monitoring for bridges, Mech. Syst. Sig. Process. 173 (2022) 108919.
[8] A.J. Hughes, L.A. Bull, P. Gardner, R.J. Barthorpe, N. Dervilis, K. Worden, On risk-based active learning for structural health monitoring, Mech. Syst. Sig. Process. 167 (2022) 108569.
[9] M.H. Soleimani-Babakamali, R. Soleimani-Babakamali, K. Nasrollahzadeh, O. Avci, S. Kiranyaz, E. Taciroglu, Zero-shot transfer learning for structural health monitoring using generative adversarial networks and spectral mapping, Mech. Syst. Sig. Process. 198 (2023) 110404.
[10] A. Entezami, H. Sarmadi, B. Behkamal, Long-term health monitoring of concrete and steel bridges under large and missing data by unsupervised meta learning, Engineering Structures 279 (2023) 115616.
[11] M.A. Pimentel, D.A. Clifton, L. Clifton, L. Tarassenko, A review of novelty detection, Signal Processing 99 (2014) 215–249.
[12] A. Deraemaeker, K. Worden, A comparison of linear approaches to filter out environmental effects in structural health monitoring, Mech. Syst. Sig. Process. 105 (2018) 1–15.
[13] A. Entezami, H. Shariatmadar, S. Mariani, Early damage assessment in large-scale structures by innovative statistical pattern recognition methods based on time series modeling and novelty detection, Adv. Eng. Software 150 (2020) 102923.
[14] A. Entezami, H. Sarmadi, B. Behkamal, A novel double-hybrid learning method for modal frequency-based damage assessment of bridge structures under different environmental variation patterns, Mech. Syst. Sig. Process. 201 (2023) 110676.
[15] S. Turrisi, A. Cigada, E. Zappa, A cointegration-based approach for automatic anomalies detection in large-scale structures, Mech. Syst. Sig. Process. 166 (2022) 108483.
[16] H. Sarmadi, A. Entezami, C. De Michele, Probabilistic data self-clustering based on semi-parametric extreme value theory for structural health monitoring, Mech. Syst. Sig. Process. 187 (2023) 109976.
[17] H. Sarmadi, K.-V. Yuen, Structural health monitoring by a novel probabilistic machine learning method based on extreme value theory and mixture quantile modeling, Mech. Syst. Sig. Process. 173 (2022) 109049.
[18] A. Fernandez-Navamuel, F. Magalhães, D. Zamora-Sánchez, Á.J. Omella, D. Garcia-Sanchez, D. Pardo, Deep learning enhanced principal component analysis for structural health monitoring, Struct. Health Monit. 21 (2022) 1710–1722.
[19] M.H. Soleimani-Babakamali, R. Sepasdar, K. Nasrollahzadeh, I. Lourentzou, R. Sarlo, Toward a general unsupervised novelty detection framework in structural health monitoring, Comput. Aided Civ. Inf. 37 (2022) 1128–1145.
[20] V. Giglioni, I. Venanzi, V. Poggioni, A. Milani, F. Ubertini, Autoencoders for unsupervised real-time bridge health assessment, Comput. Aided Civ. Inf. 38 (2023) 959–974.
[21] K. Yang, S. Kim, J.B. Harley, Unsupervised long-term damage detection in an uncontrolled environment through optimal autoencoder, Mech. Syst. Sig. Process. 199 (2023) 110473.
[22] L. Li, M. Morgantini, R. Betti, Structural damage assessment through a new generalized autoencoder with features in the quefrency domain, Mech. Syst. Sig. Process. 184 (2023) 109713.
[23] M.H. Daneshvar, H. Sarmadi, K.-V. Yuen, A locally unsupervised hybrid learning method for removing environmental effects under different measurement periods, Measurement 208 (2023) 112465.
[24] A. Diez, N.L.D. Khoa, M. Makki Alamdari, Y. Wang, F. Chen, P. Runcie, A clustering approach for structural health monitoring on bridges, J. Civ. Struct. Health Monit., 6 (2016) 429-445.
[25] L.-F. Mei, W.-J. Yan, K.-V. Yuen, W.-X. Ren, M. Beer, Transmissibility-based damage detection with hierarchical clustering enhanced by multivariate probabilistic distance accommodating uncertainty and correlation, Mech. Syst. Sig. Process. 203 (2023) 110702.
[26] M. Silva, A. Santos, R. Santos, E. Figueiredo, C. Sales, J.C.W.A. Costa, Agglomerative concentric hypersphere clustering applied to structural damage detection, Mech. Syst. Sig. Process. 92 (2017) 196–212.
[27] A. Santos, E. Figueiredo, M. Silva, R. Santos, C. Sales, J.C.W.A. Costa, Genetic-based EM algorithm to improve the robustness of Gaussian mixture models for damage detection in bridges, Struct. Contr. Health Monit. 24 (2017) e1886.
[28] A. Entezami, H. Sarmadi, B. Behkamal, C. De Michele, On continuous health monitoring of bridges under serious environmental variability by an innovative multi-task unsupervised learning method, Struct. Infrastruct. Eng., In Press (2023) 1-19.
[29] R. Langone, E. Reynders, S. Mehrkanoon, J.A. Suykens, Automated structural health monitoring based on adaptive kernel spectral clustering, Mech. Syst. Sig. Process. 90 (2017) 64–78.
[30] A. Entezami, H. Sarmadi, B. Behkamal, Short-term damage alarming with limited vibration data in bridge structures: A fully non-parametric machine learning technique, Measurement 235 (2024) 114935.
[31] Z. Wang, D.-H. Yang, T.-H. Yi, G.-H. Zhang, J.-G. Han, Eliminating environmental and operational effects on structural modal frequency: A comprehensive review, Struct. Contr. Health Monit. 29 (2022) e3073.
[32] P. Moser, B. Moaveni, Environmental effects on the identified natural frequencies of the Dowling Hall Footbridge, Mech. Syst. Sig. Process. 25 (2011) 2336–2357.
[33] D. Anastasopoulos, G. De Roeck, E.P.B. Reynders, One-year operational modal analysis of a steel bridge from high-resolution macrostrain monitoring: Influence of temperature vs, Retrofitting, Mech. Syst. Sig. Process. 161 (2021) 107951.
[34] A. Entezami, H. Sarmadi, B. Behkamal, Removal of freezing effects from modal frequencies of civil structures for structural health monitoring, Engineering Structures 319 (2024) 118722.
[35] H. Li, S. Li, J. Ou, H. Li, Modal identification of bridges under varying environmental conditions: Temperature and wind effects, Struct. Contr. Health Monit. 17 (2010) 495–512.
[36] Y. Zhou, L. Sun, Effects of environmental and operational actions on the modal frequency variations of a sea-crossing bridge: A periodicity perspective, Mech. Syst. Sig. Process. 131 (2019) 505–523.
[37] C.M. Bishop, Pattern Recognition and Machine Learning, Springer, Singapore, 2006.
[38] X. He, D. Cai, Y. Shao, H. Bao, J. Han, Laplacian Regularized Gaussian Mixture Model for Data Clustering, IEEE Trans. Knowl. Data Eng. 23 (2011) 1406–1418.
[39] A.J. Izenman, Modern Multivariate Statistical Techniques: Regression, Classification and Manifold Learning, Springer, New York, NY, US, 2008.
[40] J. Liu, D. Cai, X. He, Gaussian mixture model with local consistency, Proceedings of the AAAI Conference on Artificial Intelligence, 2010, pp. 512-517.
[41] G.J. McLachlan, T. Krishnan, The EM Algorithm and Extensions, John Wiley & Sons Inc, New Jersey, United States, 2007.
[42] W.L. Hamilton, Graph Representation Learning, Morgan & Claypool Publishers, 2020.
[43] L. Yang, A. Shami, On hyperparameter optimization of machine learning algorithms: Theory and practice, Neurocomputing 415 (2020) 295–316.

[44] M. He, W. Guo, An Integrated Approach for Bearing Health Indicator and Stage Division Using Improved Gaussian Mixture Model and Confidence Value, IEEE Trans. Ind. Inform. 18 (2022) 5219–5230.
[45] M. Walters, Small components in k-nearest neighbour graphs, Discrete Applied Mathematics 160 (2012) 2037–2047.
[46] H. Sarmadi, A. Entezami, B. Behkamal, C. De Michele, Partially online damage detection using long-term modal data under severe environmental effects by unsupervised feature selection and local metric learning, J. Civ. Struct. Health Monit. 12 (2022) 1043–1066.
[47] B. Peeters, G. De Roeck, One-year monitoring of the Z24-Bridge: Environmental effects versus damage events, Earthquake Eng. Struct. Dyn. 30 (2001) 149–171.
[48] V. Giglioni, J. Poole, I. Venanzi, F. Ubertini, K. Worden, A domain adaptation approach to damage classification with an application to bridge monitoring, Mech. Syst. Sig. Process. 209 (2024) 111135.
[49] H. Sarmadi, Investigation of machine learning methods for structural safety assessment under variability in data: Comparative studies and new approaches, Journal of Performance of Constructed Facilities 35 (2021) 04021090.
[50] V. Giglioni, E. García-Macías, I. Venanzi, L. Ierimonti, F. Ubertini, The use of receiver operating characteristic curves and precision-versus-recall curves as performance metrics in unsupervised structural damage classification under changing environment, Engineering Structures 246 (2021) 113029.
[51] C.C. Aggarwal, C.K. Reddy, Data Clustering: Algorithms and Applications, CRC Press, Boca Raton, Florida, United States, 2016.
[52] F. Gharibnezhad, L.E. Mujica, J. Rodellar, Applying robust variant of Principal Component Analysis as a damage detector in the presence of outliers, Mech. Syst. Sig. Process. 50–51 (2015) 467–479.
[53] S. Li, H. Li, Y. Liu, C. Lan, W. Zhou, J. Ou, SMC structural health monitoring benchmark problem using monitored data from an actual cable-stayed bridge, Struct. Contr. Health Monit. 21 (2014) 156–172.
[54] H. Li, Structural assessment of concrete cable-stayed bridge after replacement of closure segment: The service stage, Pract. Periodical Struct. Des. Constr. 25 (2020) 04020023.